To the Graduate Council:

I am submitting herewith a thesis written by Christopher E. Bible entitled "Destruction of Nitric Oxide in a Liquid Metal Reactor System". I have examined the final copy of this thesis for form and content and recommend that it be accepted in partial fulfillment of the requirements for the degree of Master of Science, with a major in Chemical Engineering.

Frederick E. Weber, Major Professor

We have read this thesis
and recommend its acceptance:

George C. Frazier

Robert M. Counce

Accepted for the Council:

Associate Vice Chancellor and
Dean of The Graduate School

DESTRUCTION OF NITRIC OXIDE IN A LIQUID METAL REACTOR SYSTEM

A Thesis

Presented for the

Master of Science Degree

The University of Tennessee, Knoxville

Christopher Eugene Bible

December 1998

DEDICATION

This thesis is dedicated to my wife

K. Noelle Bible

Her patience and love allowed it to be.

ACKNOWLEDGEMENTS

There are many people to whom I am grateful for making this research possible. I have benefitted greatly from interacting with research scientists and engineers in private industry whose area of expertise is catalysis and high temperature reactor systems. I am particularly greatful to my Thesis Committee, Dr. Fred Weber, Dr. Pete Counce and Dr. George Frazier for their patience and support.

I would also like to extend special gratitude to Molten Metal Technology for funding this research. I would like to thank Eric Loewen and Dr. Tom Griffin in particular, who provided me with the resources to work on this project in conjunction with other ongoing industrial research activities. Their support made this project possible.

ABSTRACT

This series of experiments was performed to demonstrate the destruction of nitric oxide in a liquid metal reactor system. Liquid metal systems consisting of molten copper, iron, zinc and tin were investigated. Gas phase injection of nitric oxide / argon mixtures into molten copper, iron, zinc and tin bath systems have been performed across a range of initial nitric oxide concentrations varying between 25-100% and temperatures of 1600°C (iron system), 1300-1600°C (copper system), 500-650°C (zinc system), and 350-750°C (tin system). Near complete (>99.8%) destruction of the nitric oxide was observed in the copper and iron systems. Destruction efficiencies exceeding 90% were observed with the tin system and destruction efficiencies approaching 50% were observed in the much cooler zinc system.

It was determined that thermal decomposition of the nitric oxide within the reactor injection lance was responsible for all of the observed destruction within the iron and copper systems. In the zinc and tin systems, reaction of the nitric oxide with the molten metal was observed. Both the reactions of the nitric oxide with the tin and zinc melts and destruction within the injection lance were responsible for all observed nitric oxide destruction in the tin and zinc melt systems.

TABLE OF CONTENTS

LIST OF TABLES

LIST OF FIGURES

NOMENCLATURE

A	Pre-exponential factor, $1/(cm^2\text{-}s)$
C_A	Concentration of species A, $moles/cm^3$
C_{AO}	Initial concentration of species A, $moles/cm^3$
C_o	Initial concentration of species *i* in the bubble, moles/liter
d_b	Diameter of the bubble, cm
d_n	Inside Diameter of the injection lance, cm
D_i	Diffusivity of species *i*, cm^2/s
D_{ij}	Diffusion coefficient for the binary mixture of species *i* and *j*, cm^2/s
Ea	Activation energy, J/mole
g	Acceleration due to gravity, $981 cm/s^2$
H	Bath height, cm
k	Reaction rate constant, $1/(cm^2\text{-}s)$ or $1/s$
Mi	Molecular weight of species *i*
Mj	Molecular weight of species *j*
$[NO]$	Concentration of nitric oxide, moles/liter
P	Pressure, atm or Power, watts
R	Universal ideal gas constant, 8.314 J/(mole-K) or Resistance, ohms
r_b	Radius of the bubble, cm
$-r_A$	Rate of disappearance of species A, $moles/(cm^3\text{-}s)$
$-r_{NO}$	Rate of consumption of NO, $moles/(liter\text{-}cm^2\text{-}s)$
T	Temperature, K
U_t	Terminal velocity of the bubble, cm/s
V	Reactor volume, cm^3
V_g	Volumetric gas flowrate, cm^3/s
v_o	Volumetric flowrate of reactant, cm^3/s

Greek Letters

α	Overall reaction order, dimensionless
ρ_l	Density of the liquid metal, g/cm^3
σ	Surface tension of the liquid metal, dynes/cm
$(\Sigma v)_i$	Atomic diffusion volume of species i
$(\Sigma v)_j$	Atomic diffusion volume of species j
τ	Residence time, s
τ_G	Characteristic time for diffusion of a gaseous species in the bubble, s
τ_{res}	Residence time, s

1. INTRODUCTION

Tanked waste from our nation's nuclear weapons production activities began to accumulate during the 1940s at various government complexes throughout the country. High level nuclear waste began to accumulate at the Hanford Nuclear Weapons complex in 1944. The Hanford waste accounts for approximately 98% of the tanked waste within the Department of Energy complex. There are currently approximately 56 million gallons of waste stored in 177 tanks on the Hanford site. The tanked wastes exist in the form of liquids, slurries, and salt cakes. Major constituents of these waste forms include sodium nitrate and sodium nitrite. Commercialization of a waste treatment system capable of successfully treating this waste remains the goal of many companies. As part of the development efforts to commercialize such a system, bench-scale research was conducted on the system's capability to destroy nitric oxide (NO). This research was undertaken due to the concerns that the large amount of $NaNO_3/NaNO_2$ in the waste might produce nitrogen oxide compounds (NO_x) in the system off-gas. Nitric oxide production within the reactor system would result in increased overall treatment cost for a full-scale treatment system.

This series of experiments was undertaken to demonstrate that the reactor system was capable of destroying nitric oxide. An investigation of the nature of the observed destruction was also undertaken. The purpose of the investigation of the nature of the reaction was to determine if the liquid metal was, in any way, catalytically enhancing the decomposition reaction.

2. LITERATURE REVIEW

Thermal and catalytically enhanced decomposition of nitric oxide has been studied extensively and a large body of information exists on the subject. Shelef and Kummer [9] have summarized data for mostly non-noble metal nitric oxide decomposition activation energies and reaction orders. Their data are shown in Table 1. The majority of the activation energy values they present lie between 70 and 132 kJ/mole. Several of the activation energy values that they present (notably the values for destruction in the CuO-I and CuO-II systems) are appreciably lower (~50 kJ/mole). These values are comparable to values reported by Winter [18] for nitric oxide decomposition over metal oxide catalysts.

Shelef [22] reported an activation energy of 84 kJ/mole for the decomposition of nitric oxide over a Pt/Al_2O_3 catalyst within a temperature range of 386-532°C at atmospheric pressure. This is significantly lower than value (132 kJ/mole) reported by Wilkstrom [16] for the decomposition of nitric oxide over a $CuO:Al_2O_3$ catalyst within a temperature range of 304-520°C at atmospheric pressure. In general, the activation energy values reported for nitric oxide decomposition over metal oxide catalysts are higher than the activation energies reported for nitric oxide decomposition over precious metals. This means that, mole for mole, the precious metal catalysts tend to be more catalytically active for the decomposition of nitric oxide.

Reported literature values for the activation energy associated with the thermal decomposition of nitric oxide lie between 63.8 kJ/mole [25] and 150 kJ/mole [24]. These values tend to be higher than the activation energy values reported for nitric oxide decomposition over either metal-oxide or precious metal catalysts.

Table 1: Literature Data for Nitric Oxide Decomposition on Various Catalysts

Catalyst	Pressure Range	NO Conc. Range	Temp. Range, ℃	Activation Energy, kJ/mole	Order of Reaction	Ref.
Quartz			>600	89.5	2	[10]
Ga_2O_3	atm	10%	<1000	80.3	0	[11]
Al_2O_3	atm	10%	<1000	132	0	
CaO	atm	10%	<1000	96.2	0	
ZrO_2	atm	10%	<1000	116	0	
Cr_2O_3	atm	10%	<1000	167-251	0	
Fe_2O_3	atm	10%	<1000	66.9	0	
ZrO_2	atm	10%	<1000	132	0	
Al_2O_3	atm	5-15%	700-1000	130	0	[12]
ZrO_2	atm	5-15%	700-1000	103	0	
Fe Oxide*	atm	0.25%	325	Not Given	Not Given	[13]
Copper Chromite*	atm	0.25%	320	Not Given	Not Given	
Supported Pt*	1-15 atm	0.4%	430-540	Not Given	2	[14]
$CuO:SiO_2$	atm	0.09%	510	163	1	[8]
Al2O3	atm	10-50%	664-807	83.7	2	[15]
$CuO:Al_2O_3(1:1)$	atm	0.072-0.22%	304-520	132	0	[16]
$CeO:Al_2O_3(1:1)$	atm	0.072-0.22%	304-520	177	0	
Cu/Zeolite	atm	4%	625-909	71-121	1	[7]
Co_3O_4	100-200 torr	100%	250-350	121	1.5-1.8	[17]
NiO	100-300 torr	100%	450-550	83.7	2	
CuO-I**	Not Given	100%	350-700	~50	2	
CuO-II***	Not Given	100%	300-450	~50	2	
Fe_2O_3	100-400 torr	100%	300-400	92.0	2	
Cr_2O_3	150-270 torr	100%	350-475	83.7	2	
ZrO_2	100-225 torr	100%	650-750	146	2	

* Commercial Catalyst
** Calcined at 700 °C in air
*** Calcined at 450 °C in air

The data published by Winter [18] concerning the activation energy of NO decomposition on thirty different metal oxides is given in Table 2. Several researchers have reported data concerning nitric oxide decomposition over noble metals, noble metal mixtures and noble metal alloys. These data are summarized in Table 3. Literature data for the thermal decomposition of nitric oxide is given in Table 4.

Table 2: Literature Data for NO Decomposition Over Oxide Catalyst

Oxide	Temperature Range, °C	Activation Energy, kJ/mole
MgO	590-760	155
NiO	430-600	126
ZnO	680-770	172
CaO	580-720	117
SrO	620-750	62.8
CuO	370-490	37.7
Al_2O_3	650-750	159
Fe_2O_3	520-660	66.9
Cr_2O_3	680-780	96.2
Ga_2O_3	610-760	121
Rh_2O_3	400-560	58.6
CeO_2	640-800	75.3
HfO_2	730-830	75.3
ThO_2	580-840	58.6
SnO_2	650-790	79.5
TiO_2	670-870	79.5
IrO_2	330-450	66.9
ScO_2	540-710	130
Y_2O_3	550-700	100
LaO_3	630-830	66.9
Nd_2O_3	580-760	105
Sm_2O_3	550-760	58.6
Eu_2O_3	550-720	96.2
Gd_2O_3	470-650	79.5
Dy_2O_3	650-760	105
Ho_2O_3	590-760	136
Er_2O_3	570-700	117
Tm_2O_3	630-760	117
Yb_2O_3	600-720	121
Lu_2O_3	540-690	109

Table 3: Literature Data for Nitric Oxide Decomposition on Noble Metal Catalyst

Catalyst	Temperature Range, °C	Pressure Range, torr	Rate Law	Activation Energy, kJ/mole	Reference
Pt	882-1403	100-500	$\frac{k[NO]}{[O_2]}$	59	[19]
Pt	1210	201-479	$\frac{k[NO]^2}{[O_2]}$	Not Given	[20]
Pt-10%Rh	1040-1390	193-477	$\frac{k[NO]^2}{[O_2]}$	113	[20]
Pt	860-1060	Not Reported	$\frac{k[NO]}{1+b[O_2]}$	92-105	[21]
Pt/Al_2O_3	386-532	760	$k[NO]^{0.95}$	84	[22]
NM-UOP	393-761	760	$k[NO]^{0.3-0.45}$	54	[22]
Pt-Ni/Al_2O_3	427-536	760-11400	$\frac{k[NO]^2}{\left(1+B\sqrt{[O_2]}\right)^2}$	Variable	[14]
Pt/Al_2O_3	600-700	10-150	$\frac{k[NO]}{1+b[O_2]}$	75	[23]
Rh_2O_3	400-560	50-400	$\frac{k[NO]}{1+b[O_2]}$	59	[18]
IrO_2	330-450	50-400	$\frac{k[NO]}{1+b[O_2]}$	67	[18]

Table 4: Literature Data for Thermal Decomposition of Nitric Oxide

Reaction	Temp Range,°C	k(T)	Units	Activation Energy, kJ/mole	Ref.
$2NO \rightarrow N_2+O_2$	1773-4573	$k_{tot}=k_{het}+k_{hom}$ $k_{het}=7x10^{12}exp(150,000/RT)$ $k_{hom}=4.8x10^{20}T^{5/2}exp(85,500/RT)$	liter/ (mole sec)	150 85.5	[24]
$2NO \rightarrow N_2+O_2$	1643-1808	$k=2.6x10^{12}exp(-63.8/RT)$	cc/ (mole sec)	63.8	[25]
$NO \rightarrow 1/2N_2+ 1/2O_2$	2473-2673	$k=3x10^{10}exp(-70,000/RT)$	liter/ (mole sec)	70	[26]
$NO \rightarrow N+O$ $N + N \rightarrow N_2$ $O+ O \rightarrow O_2$ Overall: $2NO \rightarrow N_2+O_2$	2673-7773 469-1006 469-5273	$k_1=1.711x10^{15}exp(75,450/T)$ $k_2=1.226x10^{16}exp(331.2/T)$ $k_3=3.751x10^{13}exp(-931.5/T)$	cc/ (mole sec)	627 2.8 -7.7	[27]

3. PRELIMINARY CALCULATIONS

Prior to setting up for the series of experiments, calculations were performed to ensure that the reactions and rates to be studied were not limited by equilibrium (thermodynamics) or mass transfer.

3.1 Thermodynamics

Several thermodynamic issues were of relevance to this study. Notably, the equilibrium limitations of the nitric oxide decomposition reaction (shown in equation 1), and the potential for nitric oxide reaction with the melt such as is shown in equations 2,3,4 and 5 were of concern.

$$NO \rightarrow 1/2\ N_2(g) + 1/2\ O_2(g) \quad (1)$$

$$Zn + NO(g) \rightarrow ZnO + 1/2\ N_2(g) \quad (2)$$

$$Sn + NO(g) \rightarrow SnO + 1/2\ N_2(g) \quad (3)$$

$$Cu + NO(g) \rightarrow CuO + 1/2\ N_2(g) \quad (4)$$

$$Fe + NO(g) \rightarrow FeO + 1/2\ N_2(g) \quad (5)$$

Figures 1 and 2 [1] provide free energies of reaction for the various possible reactions within the scope of this study. The calculations for free energies of reaction involving metals are for liquid-phase metal species (values are extrapolated to below-melting-point temperatures by using a Criss-Cobble technique).

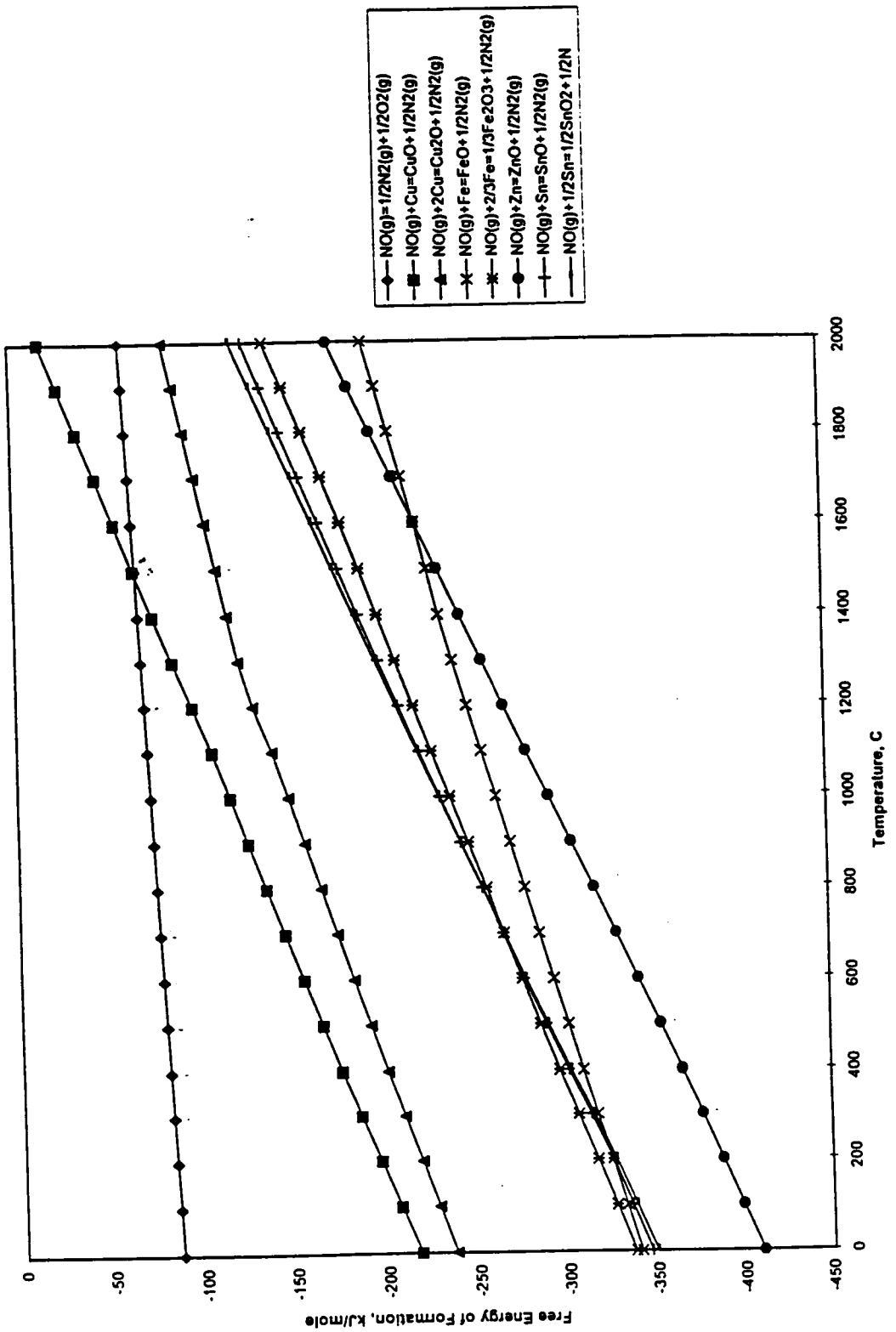

Figure 1: Free Energies of Reaction for Nitric Oxide With Bath

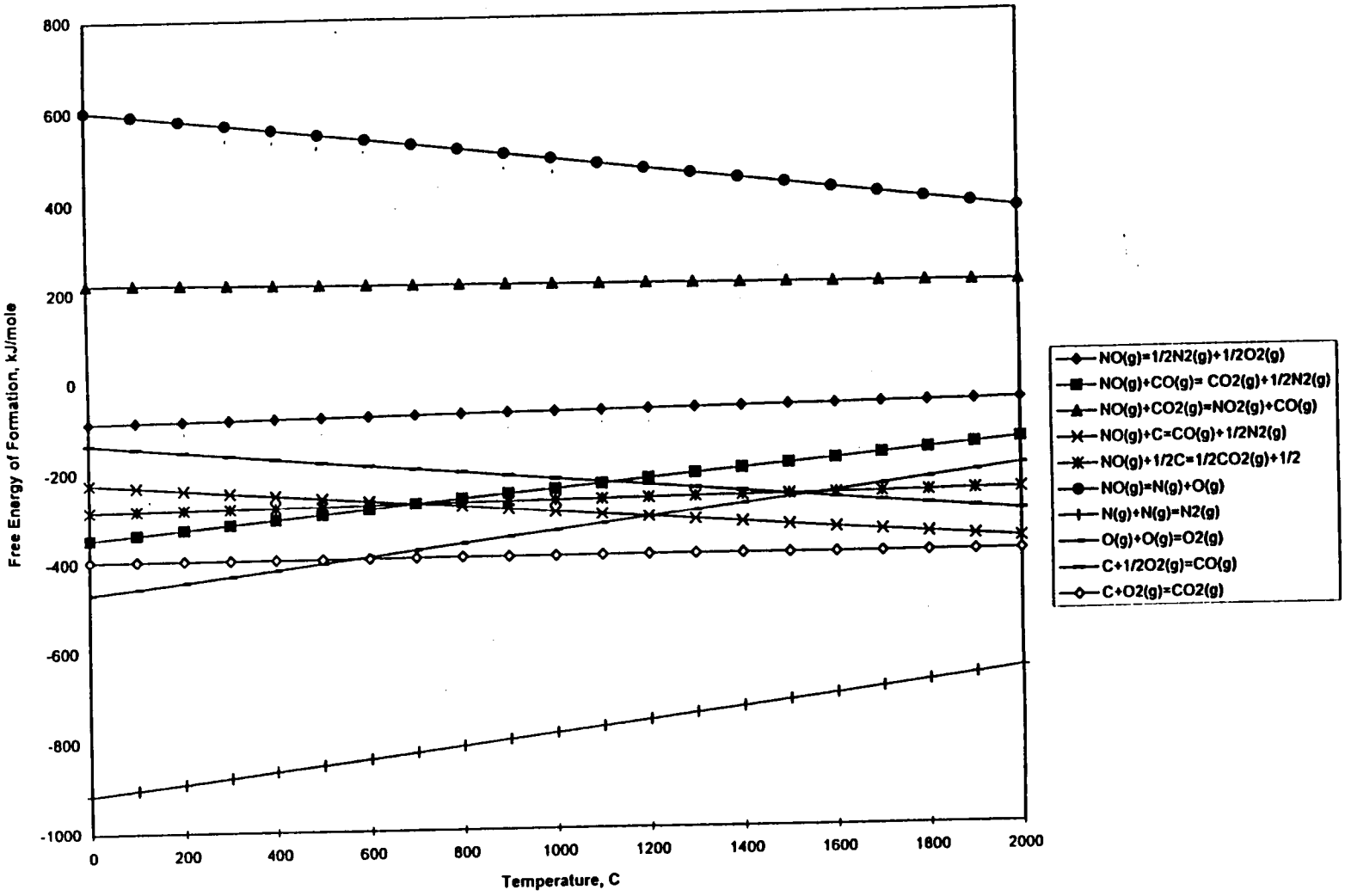

Figure 2: Free Energies of Reaction for Nitric Oxide With Other Species

As shown in Figures 1 and 2, the reaction shown in equation (1) is thermodynamically favorable within the range of temperatures used for this investigation. Figure 2 also shows that the reactions shown in equations (2)-(5) are more favorable than the reaction shown in equation (1) within the range of temperatures used for this investigation. This implies that some destruction of nitric oxide can occur through the reaction of the nitric oxide with the various molten metal baths instead of by way of catalytically enhanced decomposition.

3.2 Mass Transfer

Throughout these experiments, a mixture of nitric oxide and argon was bubbled through an alumina lance (nominal 0.25" o.d., 0.155" i.d.) beneath a liquid metal bath. In a situation where the overall nitric oxide decomposition reaction rate is limited by mass transfer of the nitric oxide to the interior of the bubble surface, diffusion of the nitric oxide to the bubble surface will be the overall rate controlling step (assuming that no thermal decomposition occurs). In order to ensure that the reactant had sufficient time to diffuse to the bubble surface, a comparison of diffusion rate to retention time was necessary. Approximating the bubbles as spheres, and assuming that the gas is stagnant, no in-bubble reaction occurs, and spherical symmetry, the conservation equation for chemical species *i* in spherical coordinates is given [3] by equation (6):

$$\frac{\partial C_i}{\partial t} = D_i \frac{1}{r^2} \frac{\partial}{\partial r}\left(r^2 \frac{\partial C_i}{\partial r} \right) \qquad (6)$$

The order of magnitude estimates of the derivatives are:

$$\frac{\partial C_i}{\partial t} \approx \frac{C_o}{\tau_G} \tag{7}$$

and

$$D_i \frac{1}{r^2} \frac{\partial}{\partial r}\left(r^2 \frac{\partial C_i}{\partial r}\right) \approx D_i \frac{C_o}{r_b^2} \tag{8}$$

therefore

$$\tau_G \approx \frac{r_b^2}{D_i} \tag{9}$$

To calculate the characteristic time for diffusion of a gaseous species in the bubble, τ_G , the bubble radius and diffusion coefficient of the gas mixture within the bubble must be determined. An empirical correlation for the diameter of an argon bubble in an iron bath is given [2] by:

$$d_b = \left[\left(\frac{6\sigma d_n}{\rho_l g}\right)^2 + \left(0.54\left(V_g \sqrt{d_n}\right)^{0.289}\right)^6\right]^{1/6} \tag{9}$$

The diffusivity of the binary mixture of argon and nitric oxide can be calculated [4] from the relationship:

$$D_{ij} = \frac{(10^{-3})T^{1.75}\left[\left(M_i + M_j\right)/M_i M_j\right]^{1/2}}{P\left[\left(\sum v\right)_i^{1/3} + \left(\sum v\right)_j^{1/3}\right]^2} \tag{10}$$

The values used for the atomic diffusion volumes [$(\Sigma v)_i$ and $(\Sigma v)_j$] are assumed to be 16.1 for argon and 17.0 for nitric oxide [4]. Assuming that terminal velocity of the bubble is reached instantaneously upon leaving the injection lance, residence time for the bubble within the bath is given by:

$$\tau_{res} = \frac{H}{U_t} \tag{11}$$

To calculate τ_{res} the bath height and the terminal velocity of the bubble must be determined. An empirical correlation for the terminal velocity of ellipsoidal bubbles is given [2] by:

$$U_t = \left[\left(2.14\frac{\sigma}{\rho_l d_b}\right) + 0.505 g d_b\right]^{1/2} \tag{12}$$

Bath height is calculated by using the known loaded metal weight and density of the liquid metal within the bath and assuming a cylindrical geometry for the melt.

To ensure that there is sufficient time for the gas to diffuse to the bubble surface, the relationship:

$$\tau_{res} > \tau_G \tag{13}$$

must be maintained throughout the experiment. During this series of experiments the data [5] in Table 5:

Table 5: Physical Properties of Liquid Metals

Metal	Surface Tension (dyne/cm)	Liquid Density (g/cm^3)
Iron	1872	7.01
Copper	1360	7.99
Zinc	782	6.57
Tin	544	7.00

was used in conjunction with equations (6)-(12) to calculate the ratio:

$$\frac{\tau_{res}}{\tau_G} \qquad (14)$$

Table 6 shows the results of these calculations for the metal systems used in this investigation. This ratio varied from 1.28 to 3.42 for these runs, thus ensuring sufficient residence time to achieve diffusion of the reactant gas to the bubble surface. For all systems studied, the ratio varied inversely with temperature. The fact that the ratio decreased with increasing temperature indicates that the effect of decreased residence time with increasing temperature was greater than the effect of increased diffusion rates with increasing temperature. Based upon these calculations, the reaction system should not have been inhibited by mass transfer of the reactant to the bubble surface.

Table 6: Ratio of Residence Time to Characteristic Diffusion Time (τ_{res}/τ_G)

System →	Fe	Cu	Zn	Sn
Temp, °C				
1600	1.30	1.28		
1500		1.33		
1400		1.38		
1300		1.44		
650			1.78	2.63
600			1.86	
550			1.93	2.77
500			2.00	
450				2.91
400				3.17
350				3.42

4. EXPERIMENTAL SETUP AND PROCEDURE

4.1 Experimental Setup

A schematic of the experimental setup is shown in Figure 3 and a detail of the reactor interior is shown in Figure 4. High pressure cylinders of high purity nitric oxide and argon were used to supply reactant gas. The gases were metered into a mixing chamber (through stainless steel tubing) using Matheson® flowmeters and then allowed to enter the reactor system via an alumina (aluminum oxide) injection lance (24" long, 0.25" od, 0.155" id).

The reactor system consisted of concentric layers of alumina crucibles (the reactor crucible was 10" tall on the exterior, 9.375" tall on the interior, 4.5" od, 3.688" id) and insulatory material sealed within a gas-tight quartz tube. The heat energy required to liqueify the metal was supplied by an Inductotherm® 75 kW power supply and induction coil. The magnetic flux created within the induction coil coupled to the carbon susceptor which increased in temperature in a manner consistent with the Joule's heating law, $P=I^2R$. The power supply was, at all times, under the control of an Omega® PID controller. Feedback to the controller was supplied by a "B"-type (Pt/Pt-Rh) thermocouple. The thermocouple was alumina sheathed and inserted into the carbon susceptor. This same thermocouple was used as a temperature indicator for the experiments. Thermal mapping experiments which have been conducted with this type of system in the past [2] have shown a less than 2% variation between the susceptor temperature and the liquid metal bath temperature. The exhaust gases were sampled by a calibrated Vacuum Technology® mass spectrometer. The mass spectrometer was accurate to ±1vol%.

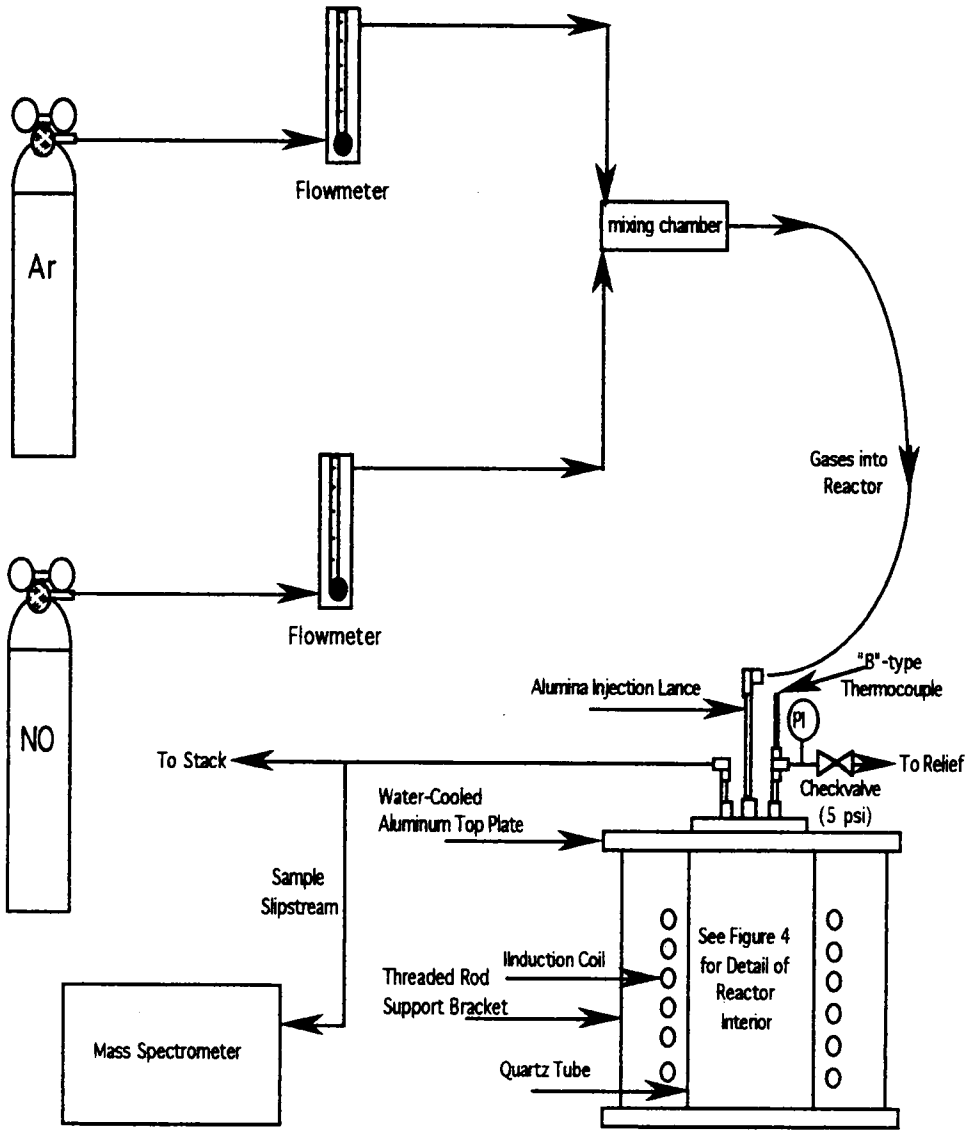

Figure 3: Schematic of Experimental Setup

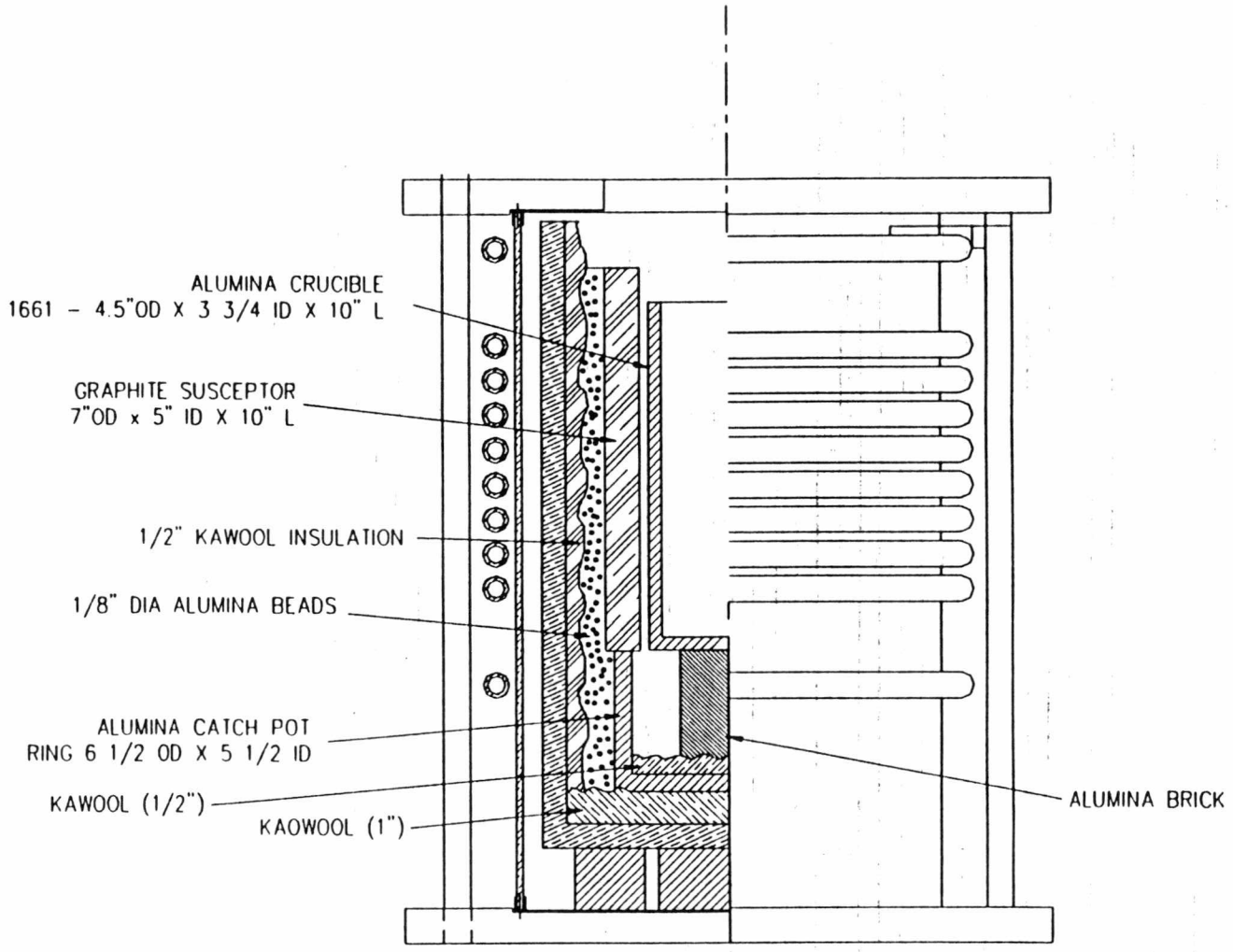

Figure 4: Detail of Reactor Interior

4.2 Experimental Procedures

The reactor was assembled (3000g of the appropriate metal was placed in the reactor crucible) and pressure tested to ensure that the system was gas-tight. The mass spectrometer was peak tuned (to ensure that the mass-spectrometer internal electronic components were observing the correct mass peaks) and baselines were established for each run.

4.2.1 Establishing Baseline on Mass-Spectrometer

A 4.0 slpm system purge with argon was initiated for approximately five minutes. After the mass spectrometer indicated that gas residuals were minimal, an analog plot of the mass-spectrometer data was saved to the data acquisition computer hard drive. This served as the zero baseline for the mass-spectrometer. 100% nitric oxide (NO) was then allowed to flow through the reactor at a rate of 2 slpm. After the mass spectrometer indicated that steady state conditions had been reached, an analog plot of the mass-spectrometer data was saved to the data acquisition computer hard drive. This was to serve as the 100% NO span for the mass-spectrometer. The 100% nitric oxide was then blended with argon to give a composition of 54/46 NO/Ar in a cold reactor. After steady state conditions were observed, a plot of the mass-spectrometer data was saved. This was to serve as the 54% NO span for the mass-spectrometer. The NO/Ar mix was further diluted to 29/71 NO/Ar. After steady state conditions were observed, a plot of the mass-spectrometer data was saved. This was to serve as the 29% NO span for the mass-spectrometer. A 4 slpm Ar purge was initiated through the reactor system and reactor heatup (at a rate not exceeding 200°C/hr.) was initiated.

4.2.2 Procedures for Injection

Once adequate baselines had been established within the reactor system and the reactor had achieved a steady-state temperature condition, nitric oxide/argon mixtures were injected into the reactor system. The injections took place both before and after a molten condition of the metal in the reactor crucible had been established. A total gas injection rate of 2 slpm was used for all experiments involving a copper or iron bath, and a total injection rate of 1 slpm was used for all tin and zinc experiments. The initial concentrations of nitric oxide in argon were varied for each melt system as shown in Table 7.

Table 7: Initial Concentration of Nitric Oxide in Argon for Different Melt Systems

Melt System	Initial NO Concentration Investigated
Iron	100%, 54%, 29%
Copper	100%, 54%, 29%
Zinc	100%, 50%, 25%
Tin	100%, 50%, 25%

5. RESULTS

Nitric oxide of various concentrations was injected into various melt systems (iron, copper, zinc and tin). Steady state reactor conditions were observed by noting the decrease in fluctuations of the nitric oxide primary and secondary peaks on the mass spectrometer. When the peak heights reached a steady value, steady state conditions were assumed to be established. The trend of increasing destruction with increasing temperature was demonstrated in all four systems. The trend of increasing destruction with increasing inlet concentration of nitric oxide is also apparent, to varying degrees, within each system. A summary of the nitric oxide destruction data obtained from the three runs is given in Table 8. Figures 5, 6, 7 and 8 present the tabular destruction data in graphical form. An overlay of the nitric oxide destruction curves (with initial concentration of 100%) for each melt system is given in Figure 9.

The nitric oxide began to thermally decompose very early during the runs. At a temperature of about 750°C (iron and copper runs), the nitric oxide % destruction began to rapidly increase. At a reactor temperature of 1600°C, >99.4% destruction of the nitric oxide was observed during injection.

The overall shape of the curves in Figures 5, 6 and 8 is in good agreement with the shapes of destruction curves observed in other catalytic systems. The cooler region on these curves (T<750°C for Figures 5 and 6) represents the reaction conditions in which insufficient energy is available within the system to overcome the activation energy "hump". The region of the curves in which destruction rates are rapidly increasing (700°C<T<1000°C) represent the reaction conditions in which activation energy limitations have been overcome.

Table 8: Nitric Oxide Destruction Data for Iron, Copper, Zinc and Tin Baths

Temp. (°C)	% NO in inlet[1]	Total Gas Flowrate[2]	% NO Destroyed Fe Bath	% NO Destroyed Cu Bath	% NO Destroyed Zn Bath	% NO Destroyed Sn Bath
Ambient	100	1 or 2 slpm	0.00%	0.00%	0.00%	—
	54 or 50	1 or 2 slpm	0.00%	0.00%	0.00%	—
	29 or 25	1 or 2 slpm	0.00%	0.00%	0.00%	—
250	100	2 slpm	6.51%	12.87%	—	—
	54	2 slpm	16.94%	21.19%	—	—
	29	2 slpm	3.46%	4.14%	—	—
350	100	1 slpm	—	—	—	41.0%
	50	1 slpm	—	—	—	47.0%
	25	1 slpm	—	—	—	41.0%
400	100	1 slpm	—	—	—	45.0%
	50	1 slpm	—	—	—	53.0%
	25	1 slpm	—	—	—	45.0%
450	100	1 slpm	—	—	—	49.0%
	50	1 slpm	—	—	—	51.0%
	25	1 slpm	—	—	—	45.0%
500	100	1 or 2 slpm	4.83%	9.79%	8.00%	—
	54 or 50	1 or 2 slpm	14.82%	16.63%	9.40%	—
	29 or 25	1 or 2 slpm	6.86%	-2.73%	0.00%	—
550	100	1 slpm	—	—	40.70%	77.0%
	50	1 slpm	—	—	28.50%	83.0%
	25	1 slpm	—	—	33.60%	79.0%
600	100	1 slpm	—	—	48.50%	—
	50	1 slpm	—	—	40.10%	—
	25	1 slpm	—	—	16.80%	—
650	100	1 slpm	—	—	29.70%	89.0%
	50	1 slpm	—	—	30.90%	92.0%
	25	1 slpm	—	—	30.40%	94.0%
750	100	2 slpm	21.69%	24.62%	—	—
	54	2 slpm	44.53%	24.66%	—	—
	29 or 25	2 slpm	37.53%	21.24%	—	97.0%
1000	100	2 slpm	90.14%	92.07%	—	—
	54	2 slpm	93.22%	95.60%	—	—
	29	2 slpm	93.80%	96.99%	—	—
1250	100	2 slpm	99.81%	—	—	—
	54	2 slpm	97.52%	—	—	—
	29	2 slpm	97.81%	—	—	—
1300	100	2 slpm	—	99.83%	—	—
(not in melt)	54	2 slpm	—	99.82%	—	—
	29	2 slpm	—	99.81%	—	—
1300	100	2 slpm	—	99.82%	—	—
(in melt)	54	2 slpm	—	99.70%	—	—
	29	2 slpm	—	99.66%	—	—
1400	100	2 slpm	—	99.80%	—	—
(in melt)	54	2 slpm	—	99.78%	—	—
	29	2 slpm	—	99.68%	—	—
1500	100	2 slpm	—	99.89%	—	—
(in melt)	54	2 slpm	—	99.76%	—	—
	29	2 slpm	—	99.74%	—	—
1600	100	2 slpm	99.47%	—	—	—
(not in melt)	54	2 slpm	99.81%	—	—	—
	29	2 slpm	99.06%	—	—	—
1600	100	2 slpm	99.56%	99.84%	—	—
(in melt)	54	2 slpm	99.73%	99.77%	—	—
	29	2 slpm	99.83%	99.63%	—	—

[1] Zinc and tin runs had 100%, 50% and 25% initial NO inlet concentration iron and copper runs had 100%,, 54% and 29%

[2] All zinc and tin runs had 1 slpm total gas flowrate; iron and copper runs had 2 slpm total gas flowrate

--- No Data

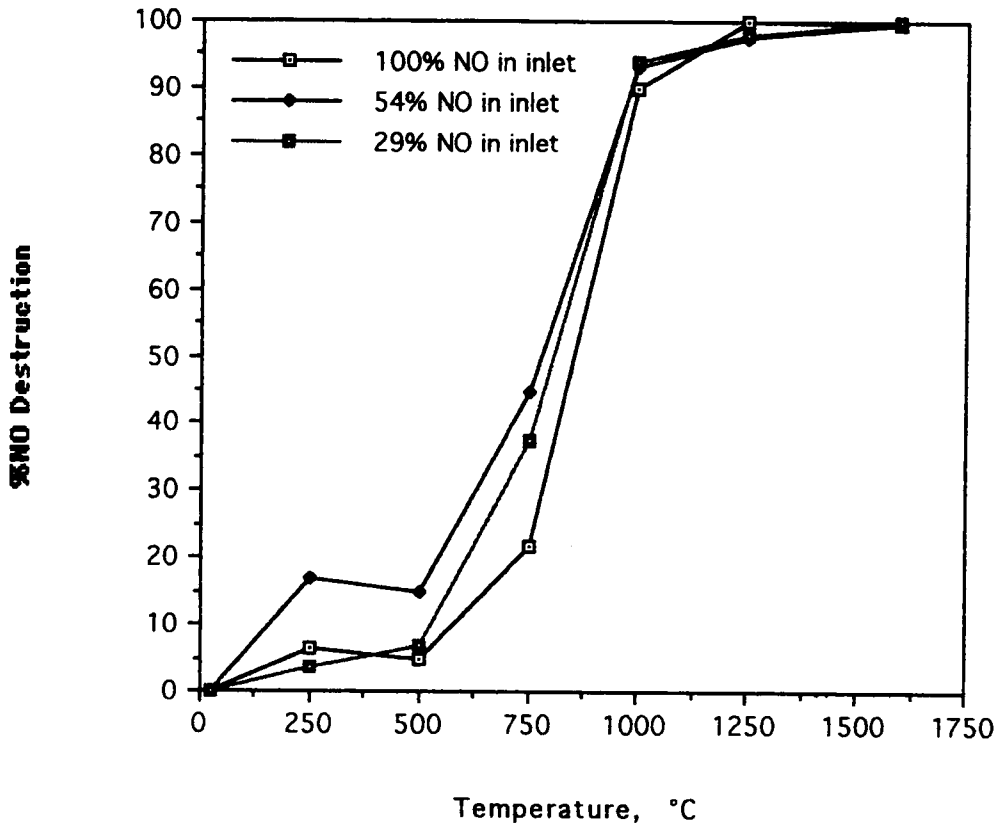

Figure 5: Nitric Oxide Destruction in Iron System
(The iron used for these experiments had a melting point of ~1600°C)

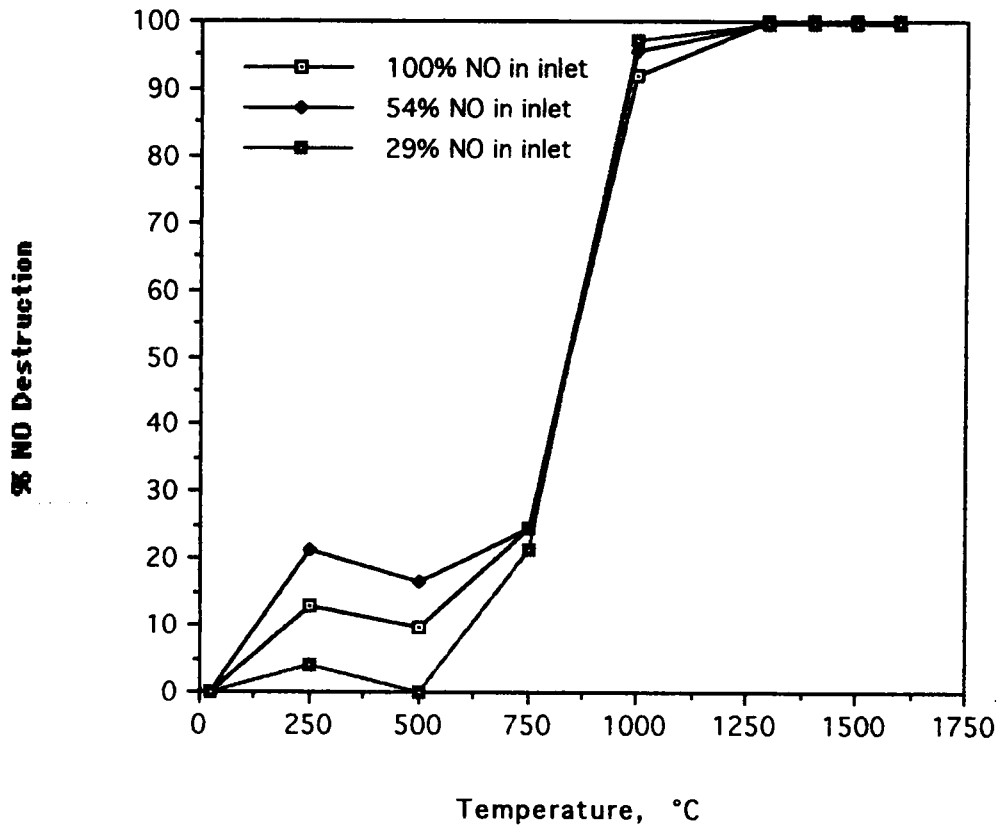

Figure 6: Nitric Oxide Destruction in Copper System
(The copper used for these experiments had a melting point of ~1083°C)

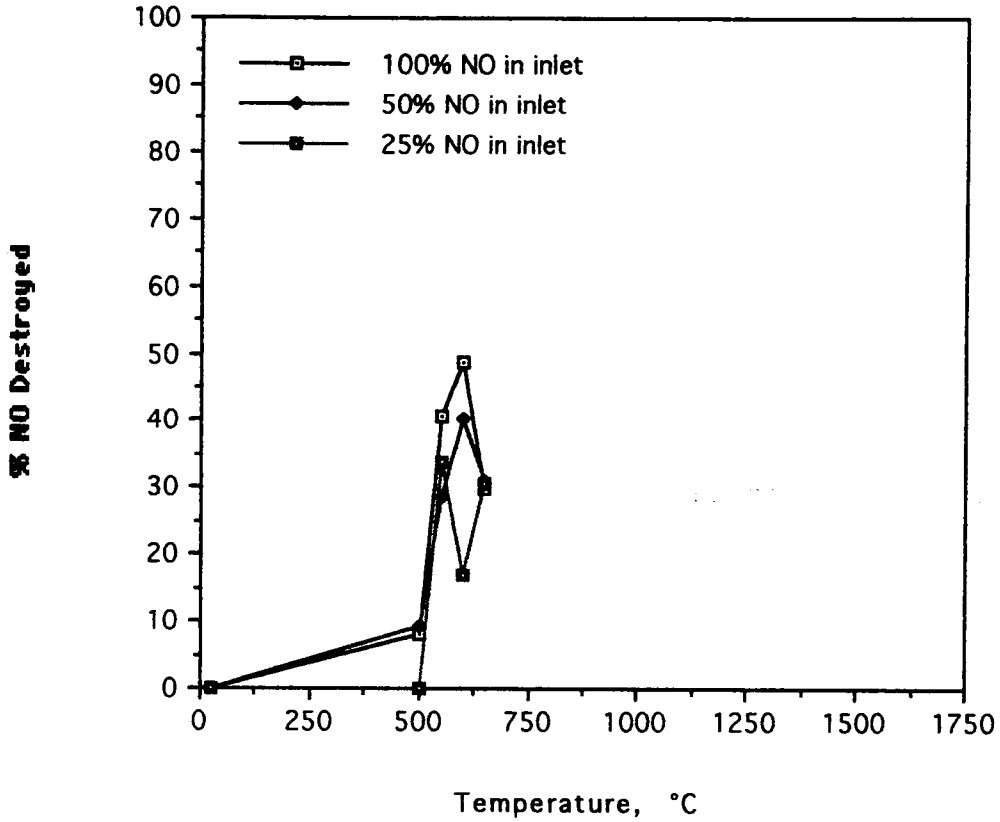

Figure 7: Nitric Oxide Destruction in Zinc System
(The zinc used for these experiments had a melting point of ~420°C)

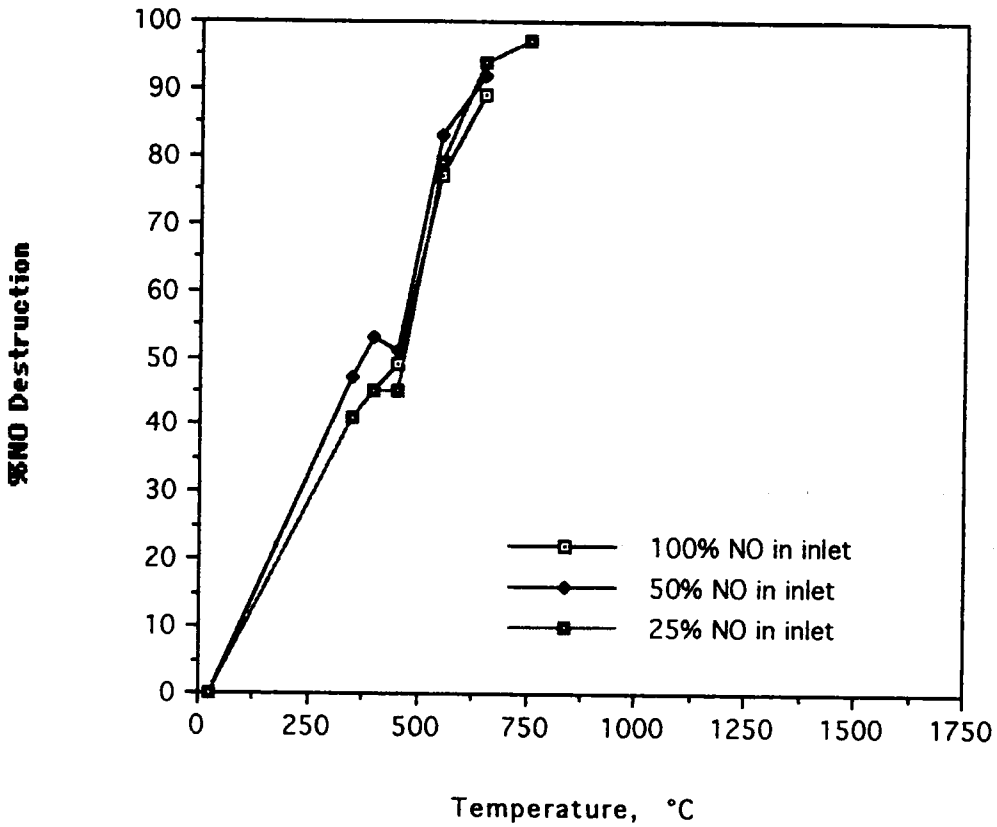

Figure 8: Nitric Oxide Destruction in Tin System
(The tin used for these experiments had a melting point of ~232°C)

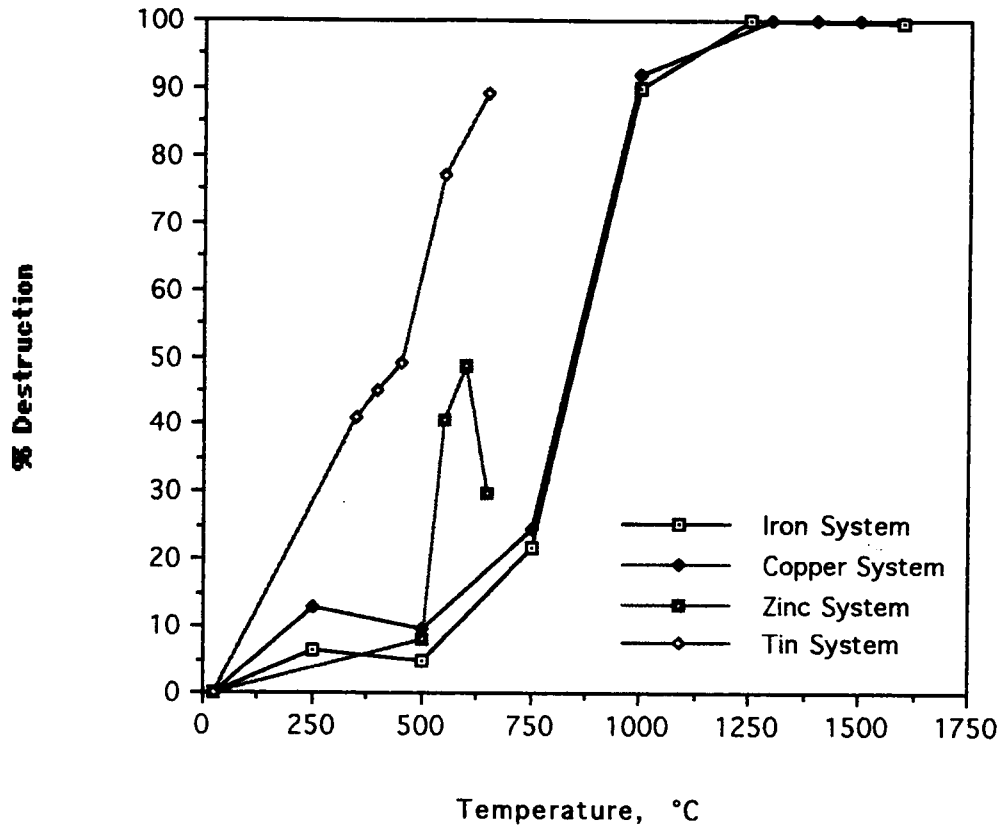

Figure 9: Overlay of 100% NO in Inlet Destruction Data

The shape of the curves in the zinc system (Figure 7) are not what is to be expected from a typical catalytic reaction system. The absence of an area in which a large increase in destruction was noted with only a small increase in temperature is strong evidence to suggest that no catalytically enhanced reaction is occurring within this system. It is possible that the lower temperatures required for this run made it impossible for the nitric oxide to overcome the activation energy limitations.

There were also anomalies with the zinc data taken at a temperature of 650°C and with the data point for 25% nitric oxide feed concentration at a temperature of 600°C. The % destruction of nitric oxide should not have decreased with increasing temperature. Bubbling within the melt began to weaken just before the 25% nitric oxide at 600°C data point was taken. It is possible that by the time these data points were taken (the 650°C points were taken last) the bath levels of zinc oxide had increased to such a level as to adversely affect the ability of the melt to break apart the nitric oxide.

6. CALCULATIONS

6.1 Reaction Order and Rate Constant Calculations

The amount of a selected component, A being converted or produced per unit time per unit quantity of a reference variable, y, in a chemically reacting system is defined [4] as the rate of reaction, r_A and:

$$r_A = \frac{1}{y}\frac{dN_A}{dt} \tag{15}$$

By definition, r_A is negative if A refers to a reactant and it is positive if it refers to a product. The reference variable, y, in homogenous fluid reactions is usually the volume of reacting fluid within the system. If the volume remains constant, equation (15) is simplified to:

$$r_A = \frac{dC_A}{dt} \tag{16}$$

where C_A is the concentration of component A. In terms of reacting components, the rate expression for a simple, irreversible reaction is given by:

$$-r_A = kC_A^a C_B^b C_C^c \ldots C_N^n \tag{17}$$

The proportionality constant, k, in equation (17) varies markedly with temperature and is called the "specific reaction rate" or the "rate constant". The overall order of reaction is defined as the sum of the exponents in equation (17). The reaction order is the molecularity (i.e. the number of molecules actually taking part in the reaction) only for elementary reactions. In the case of an elementary reaction, the reaction rate equation can be derived directly from the stoichiometric equation since the stoichiometric equation describes the true reaction mechanism. Assumption of an elementary form for a decomposition reaction is usually valid [6]. For the nitric oxide system, the elementary form is given by:

$$-r_{NO}=k[NO]^{\alpha} \quad (18)$$

The rate equation is linearized by taking natural logarithms of both sides and simplifying:

$$\ln(-r_{NO}) = \ln k + \alpha \ln([NO]) \quad (19)$$

Equation (19) shows that by plotting $\ln(-r_{NO})$ vs. $\ln([NO])$ the overall reaction order, α, is given by the slope of the line. The natural logarithm of the reaction rate constant is given by the intercept. Experimental destruction data as a function of nitric oxide inlet concentration at a constant temperature and pressure are used to generate these plots (i.e. inlet concentrations were varied at constant temperatures). Parameters which were used to evaluate the total surface area of the reactant mixture which was exposed to the molten metal during a particular experiment are shown in Table 9. Values of α and k obtained for each melt system are presented in Table 10. The plots are given in Figures 10-23.

Table 9: Calculated Parameters Used For Reaction Rate Constant Determinations

Melt System	Temp., °C	Bubble Diameter, cm	Temperature Corrected Flowrate, cc/s	Residence Time In Melt, s	Surface Area of Bubbles in Melt, cm^2
Fe	1600	2.21	209.5	0.187	106
Cu	1600	2.21	209.5	0.170	96.4
	1500	2.18	198.3	0.171	93.6
	1400	2.14	187.1	0.172	90.4
	1300	2.10	176.0	0.174	87.1
Zn	650	1.48	51.6	0.218	45.6
	600	1.45	48.8	0.219	44.1
	550	1.43	46.0	0.220	42.5
	500	1.40	43.2	0.221	40.8
Sn	650	1.48	51.6	0.212	44.4
	550	1.43	46.0	0.214	41.4
	450	1.38	40.4	0.217	38.2
	400	1.35	37.6	0.218	36.6
	350	1.32	34.8	0.220	34.9

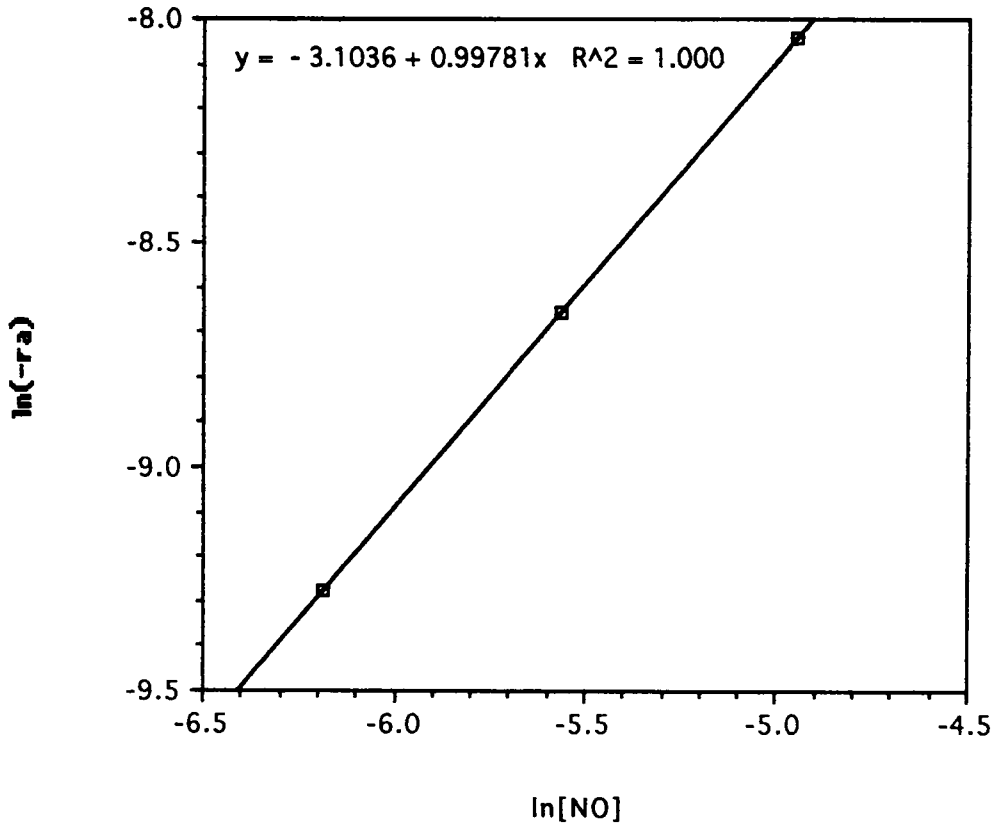

Figure 10: Iron System 1600°C Rate Order and Rate Constant Determination

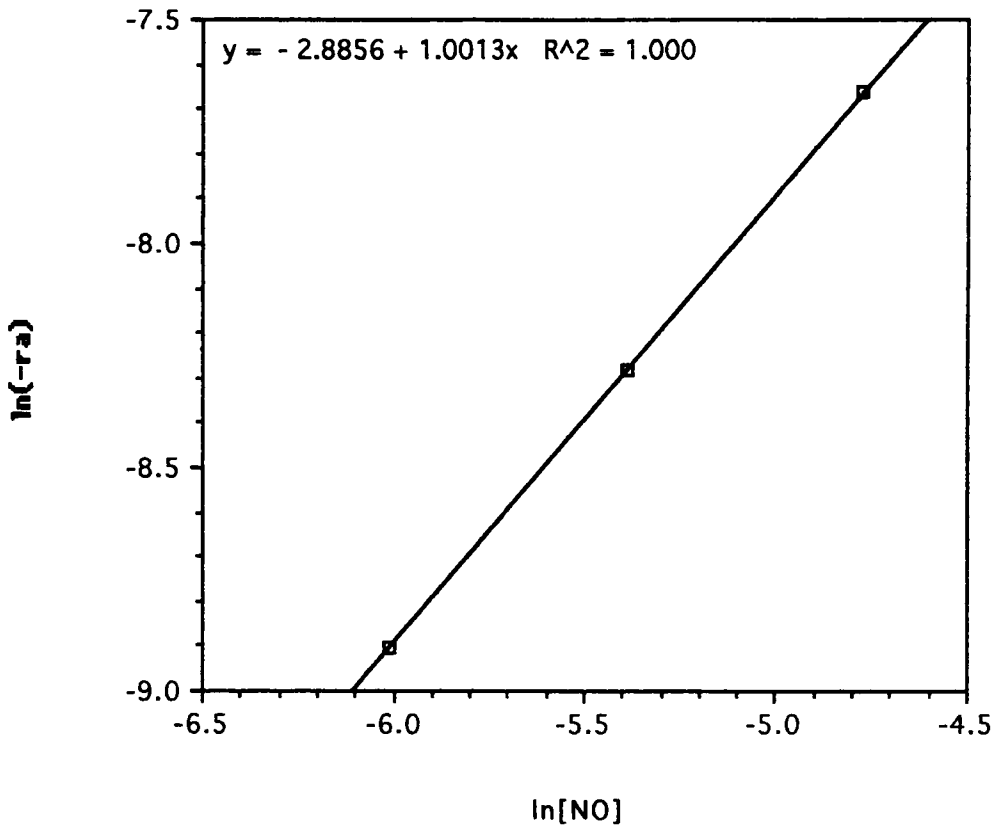

Figure 11: Copper System 1300°C Rate Order and Rate Constant Determination

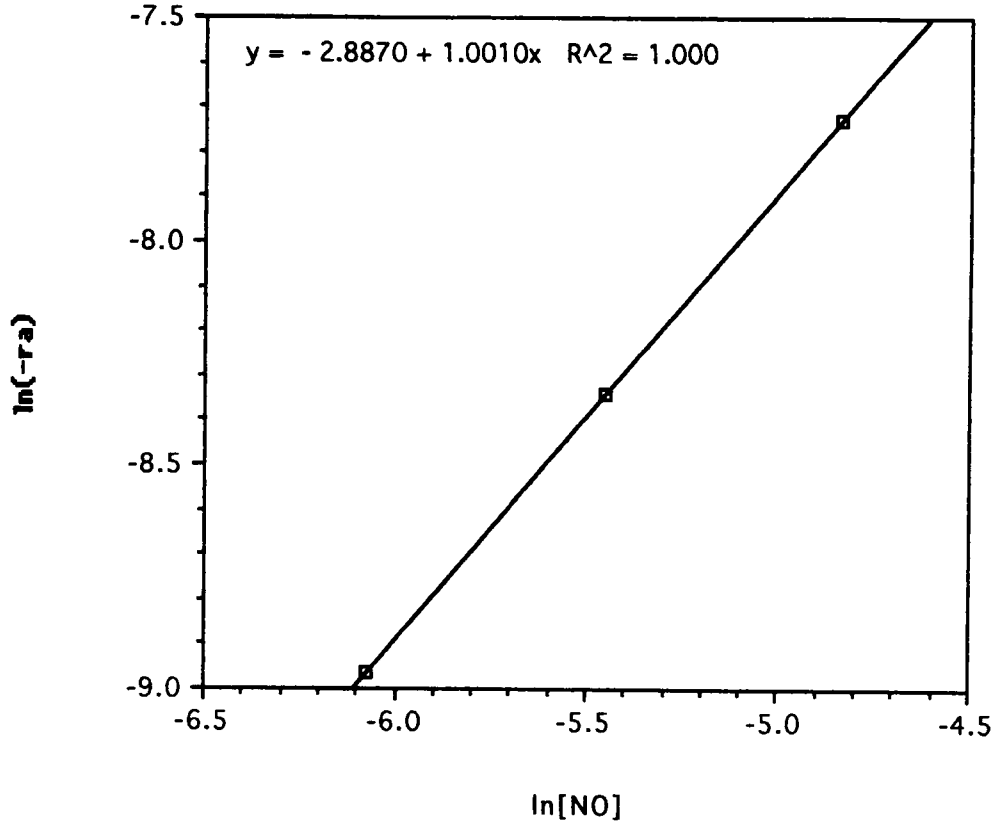

Figure 12: Copper System 1400°C Rate Order and Rate Constant Determination

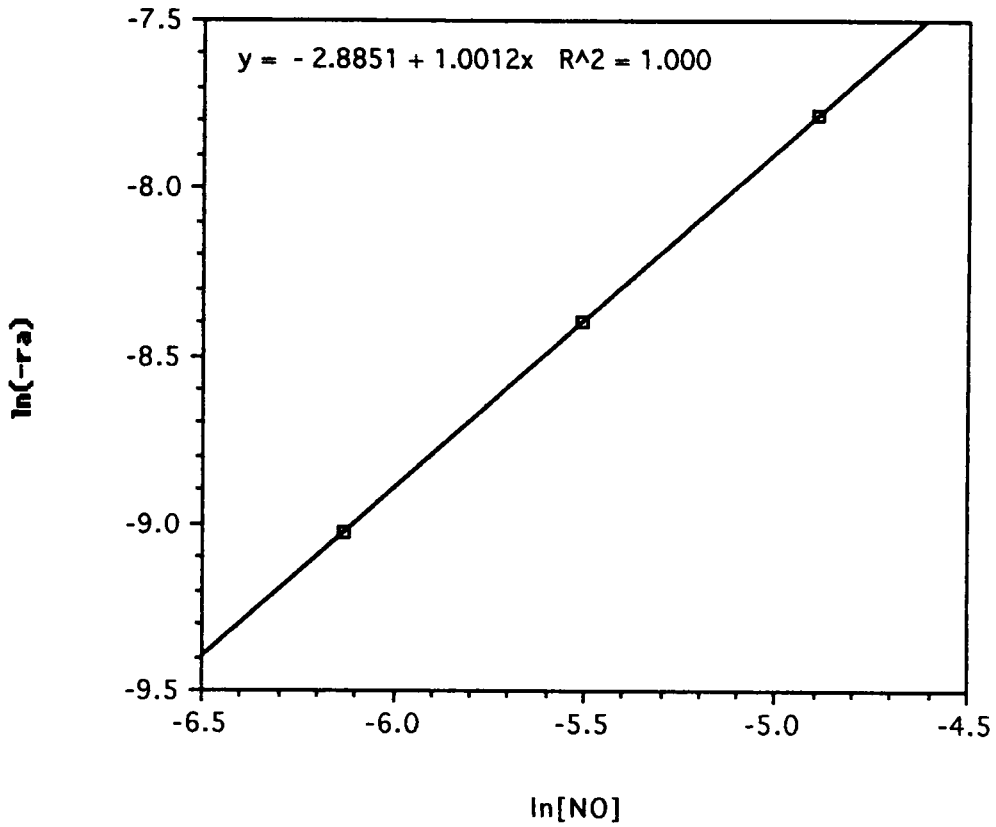

Figure 13: Copper System 1500°C Rate Order and Rate Constant Determination

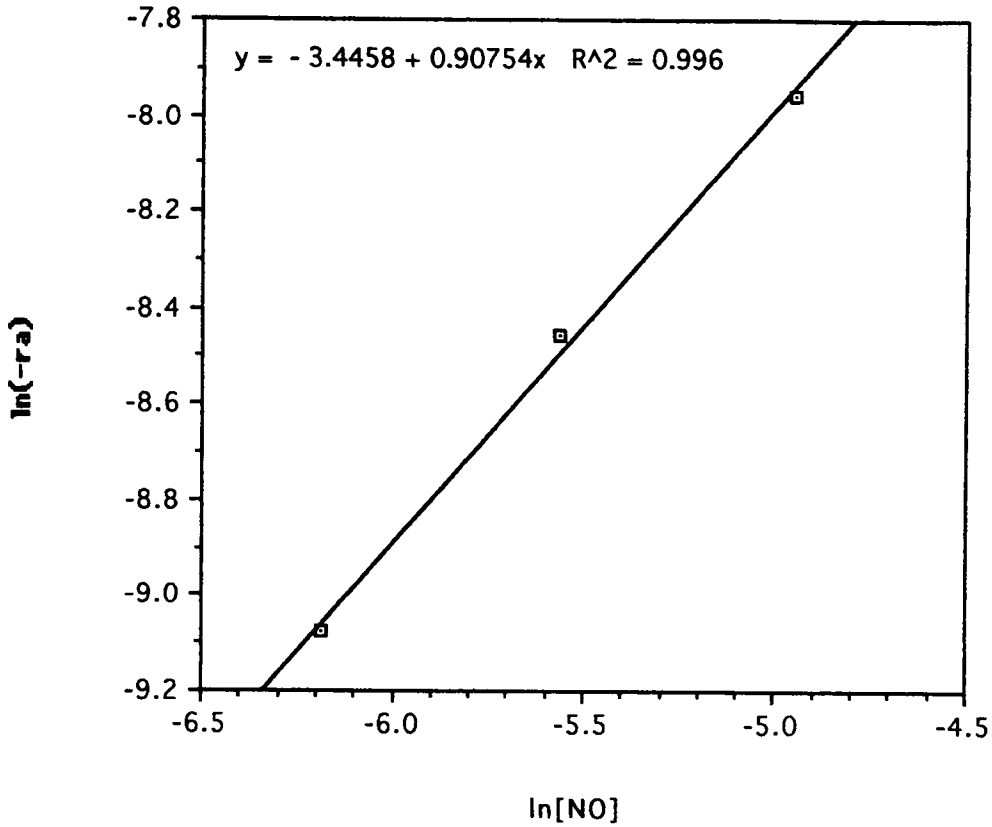

Figure 14: Copper System 1600°C Rate Order and Rate Constant Determination

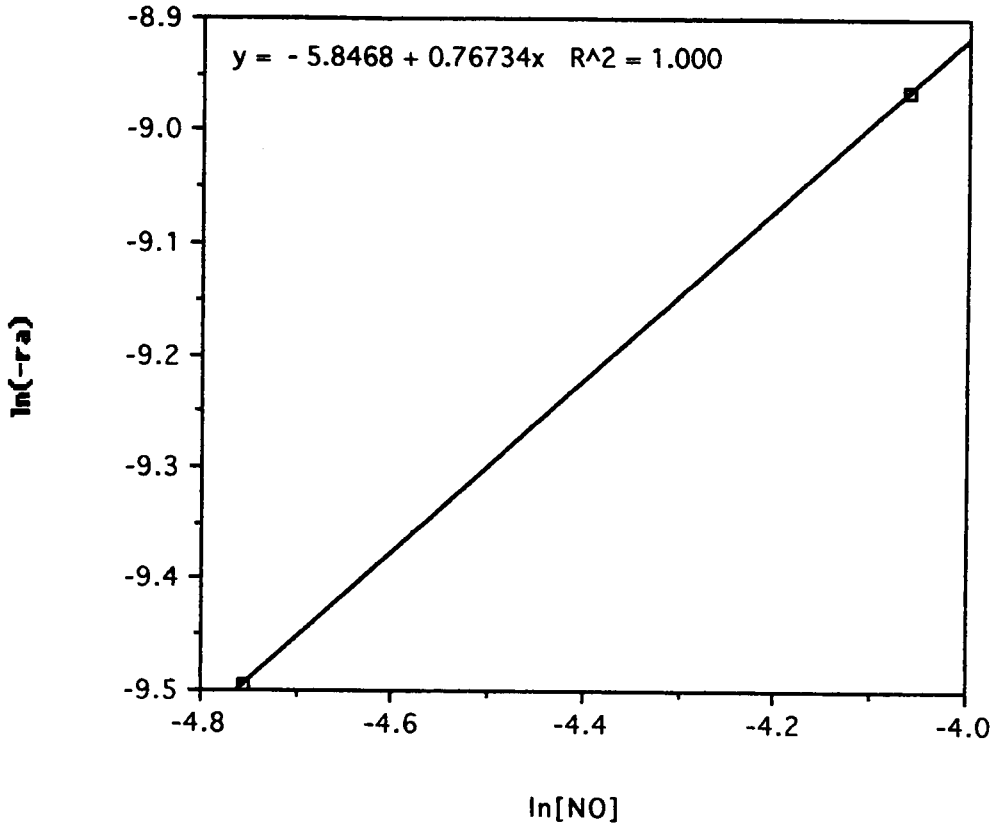

Figure 15: Zinc System 500°C Rate Order and Rate Constant Determination

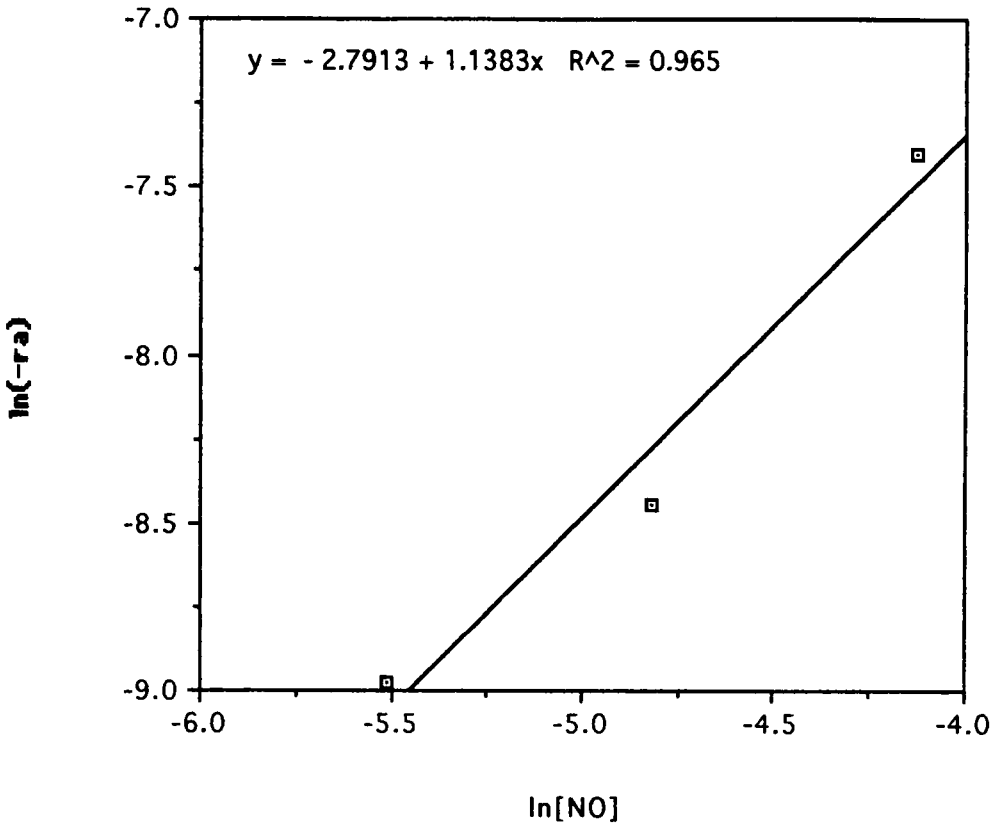

Figure 16: Zinc System 550°C Rate Order and Rate Constant Determination

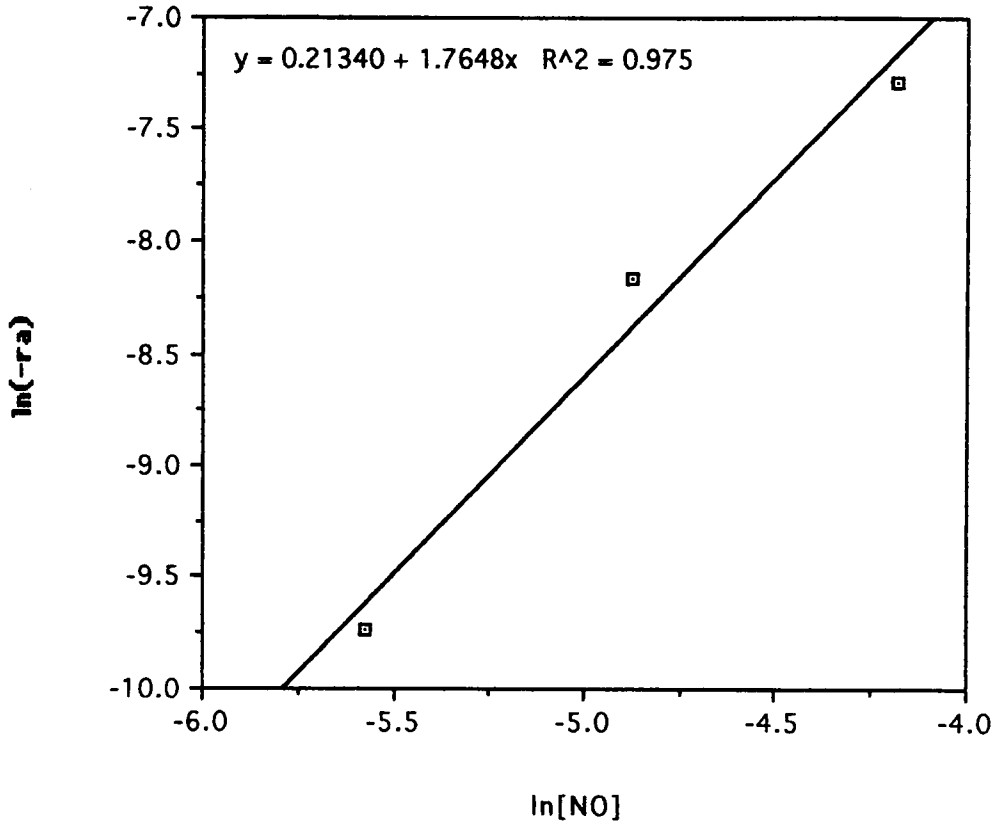

Figure 17: Zinc System 600°C Rate Order and Rate Constant Determination

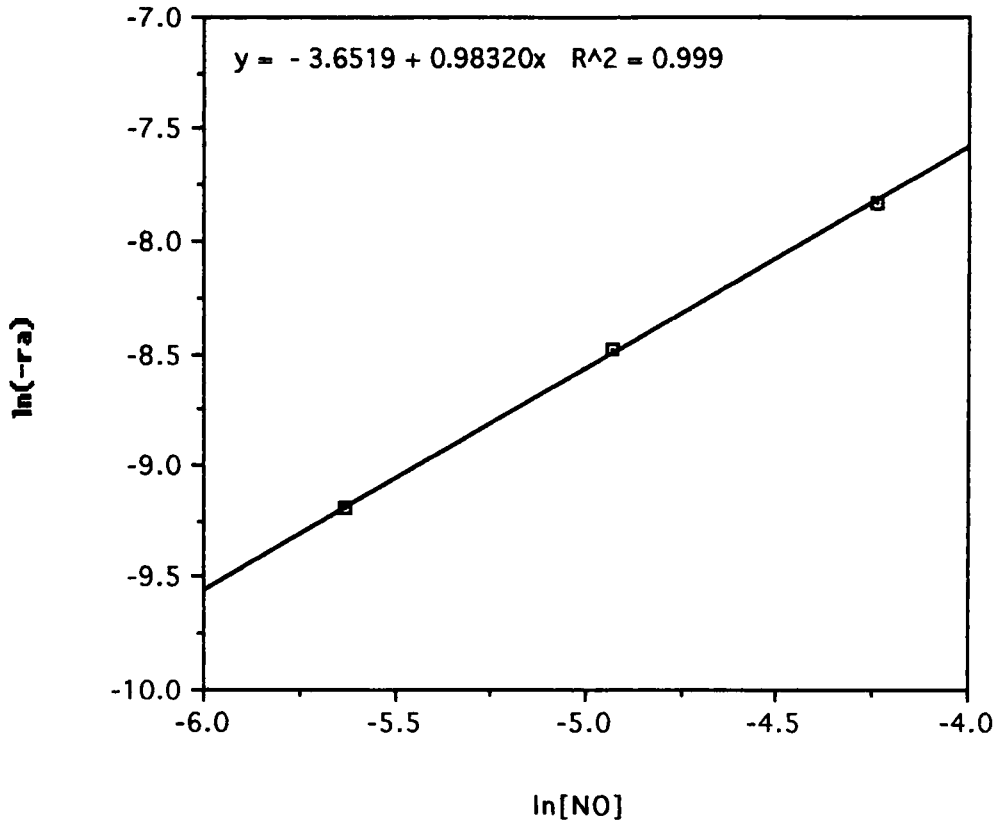

Figure 18: Zinc System 650°C Rate Order and Rate Constant Determination

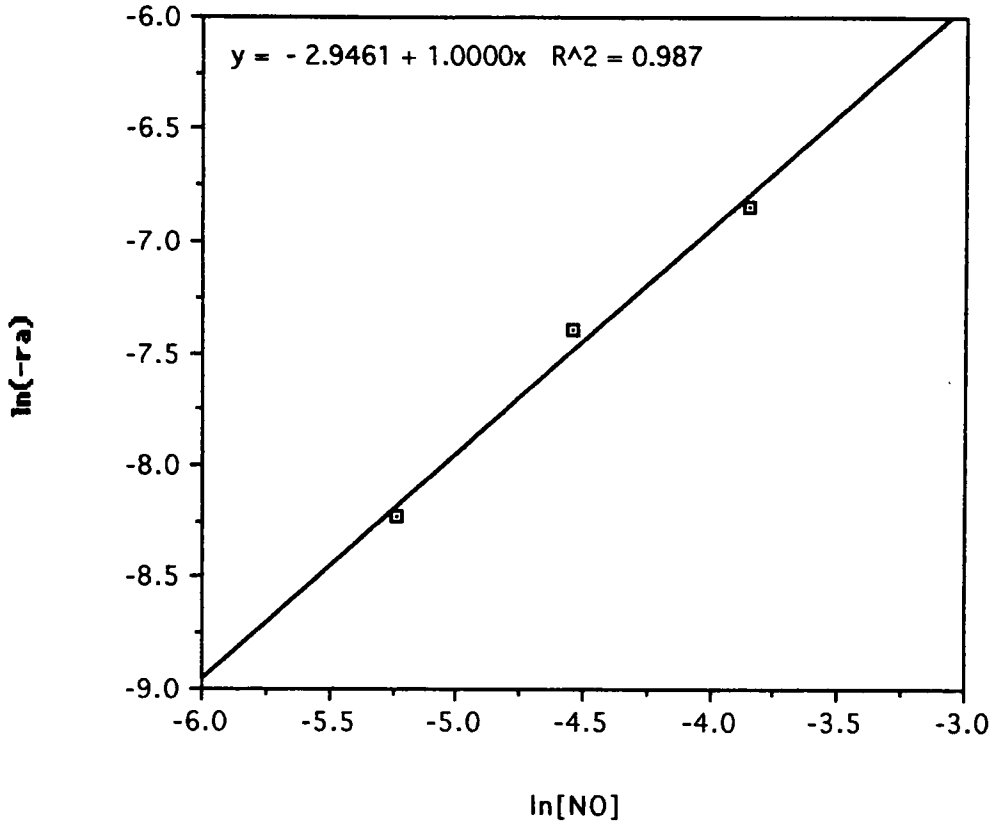

Figure 19: Tin System 350°C Rate Order and Rate Constant Determination

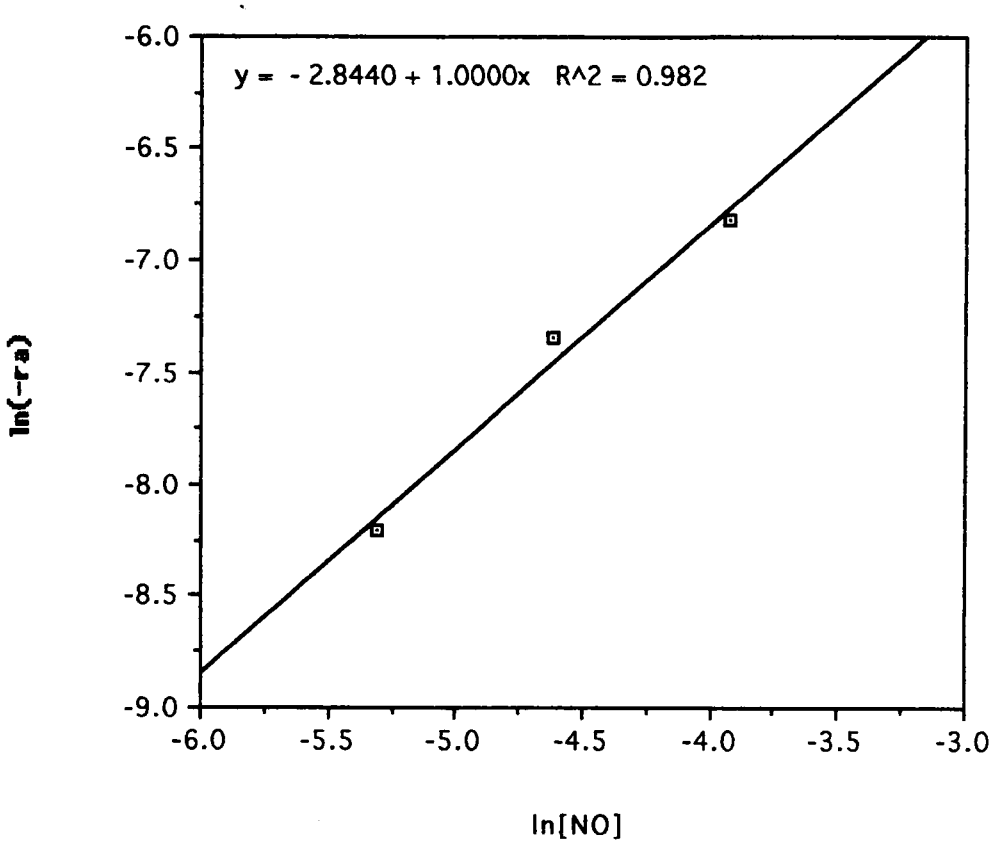

Figure 20: Tin System 400°C Rate Order and Rate Constant Determination

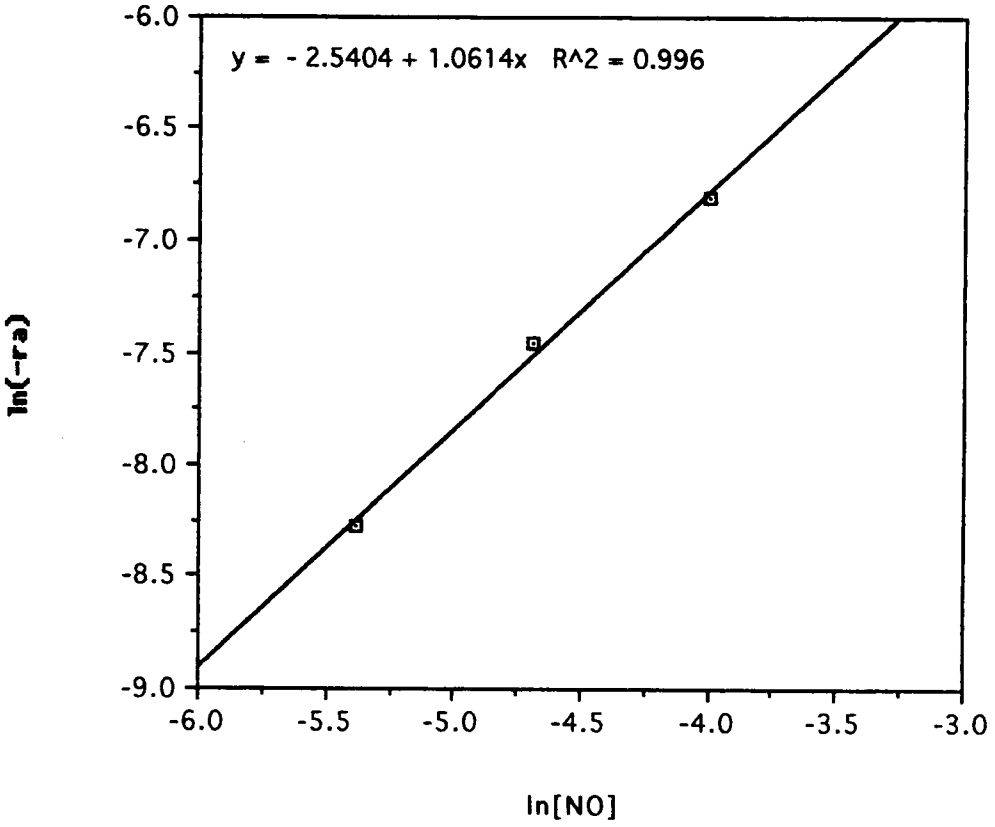

Figure 21: Tin System 450°C Rate Order and Rate Constant Determination

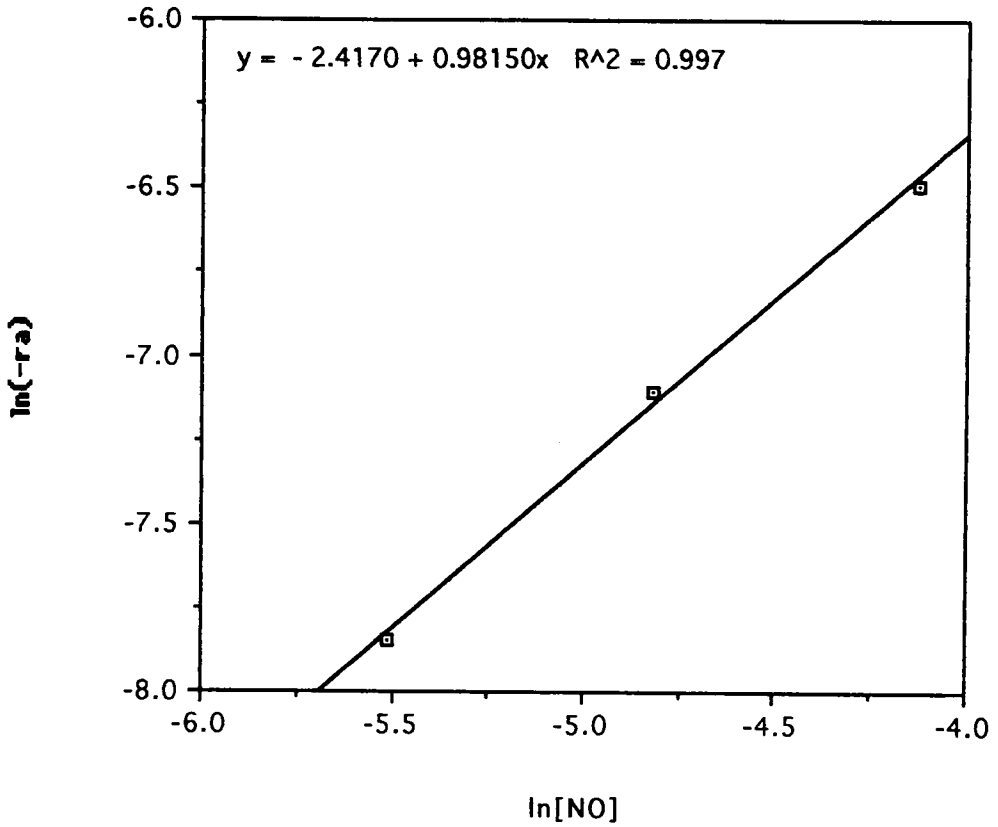

Figure 22: Tin System 550°C Rate Order and Rate Constant Determination

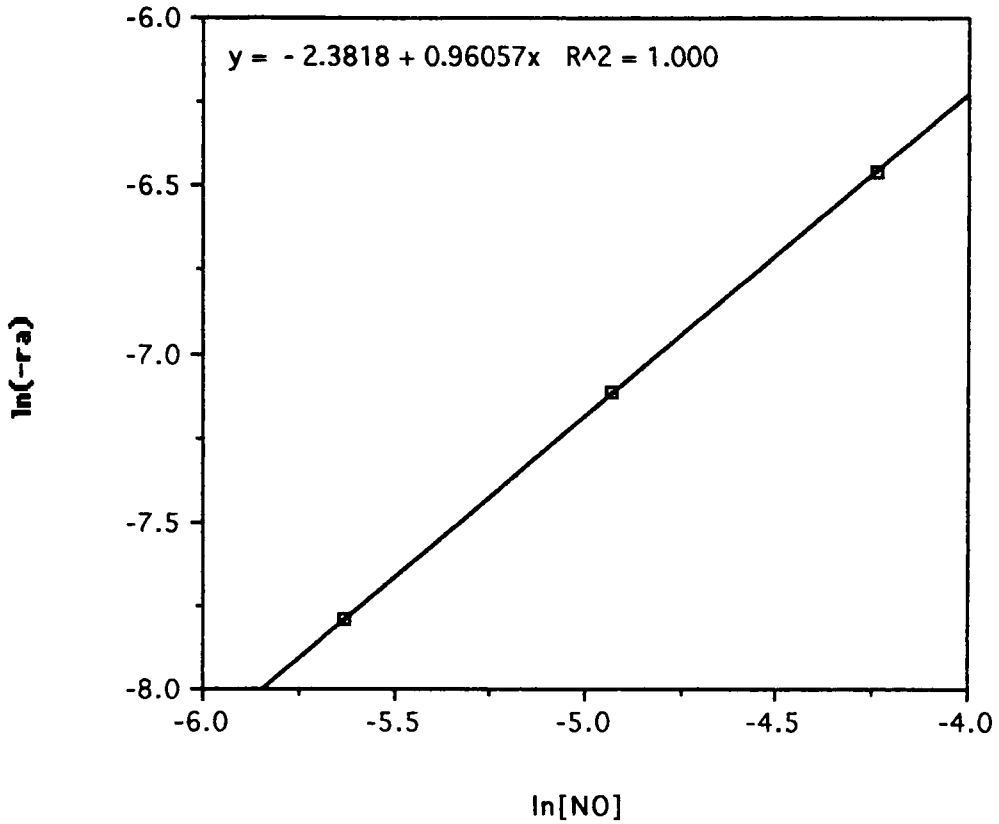

Figure 23: Tin System 650°C Rate Order and Rate Constant Determination

Table 10: Experimentally Determined Reaction Order and Rate Constants Summary

System & Temperature, °C	Overall Reaction Order, α	Reaction Rate Constant, k	Correlation Coefficient, r^2
Fe			
1600	1.0	0.045	1.0
Average	**1.0**		
Cu			
1300	1.0	0.056	1.0
1400	1.0	0.056	1.0
1500	1.0	0.056	1.0
1600	0.9	0.032	1.0
Average	**0.98**		
Zn			
500	0.77	0.0029	1.0
550	1.1	0.061	0.97
600	1.8	1.2	0.98
650	0.98	0.026	1.0
Average	**1.2**		
Sn			
350	1.0	0.052	0.99
400	1.0	0.058	0.98
450	1.1	0.079	1.0
550	0.98	0.089	1.0
650	0.96	0.093	1.0
Average	**1.0**		

The overall reaction order appears to be one (1) except in the case of the zinc melt system. This implies that the overall reaction rate can be given by:

$$-r_A = k[NO] \qquad (20)$$

The anomalous results for the zinc system are most likely attributable to the fact that zinc is highly reactive toward nitric oxide. The results are in agreement with results obtained by Li and Hall [7] as well as Sourirajan and Blumenthal [8]. Their results were obtained for solid phase copper/zeolite and copper/silica systems respectively.

6.2 Activation Energy Determination

Lowering of the system activation energy is the criteria for demonstration of the catalytic nature of the melt system [6]. Activation energy is related to the reaction rate constant through the Arhennius equation:

$$k = Ae^{-Ea/RT} \tag{21}$$

Equation (21) can be linearized and simplified using natural logarithms to yield:

$$\ln k = \ln A + (-E_a/R)1/T \tag{22}$$

This means that a plot of lnk vs. 1/T should yield a straight line with slope ($-E_a/R$). The experimental data (shown in Table 10) for the copper, zinc and tin systems are plotted in this fashion (there was insufficient data to generate an activation energy plot for the iron system) and are shown in Figures 24-26. A summary of the results is given in Table 11.

The experimentally determined activation energy of -39 kJ/mole for the copper system is obviously incorrect and meaningless. This error is most likely attributable to the fact that the nitric oxide was possibly thermally decomposing within the hot alumina injection lance as it traveled through the heated region of the lance and into the melt. This is likely also true for the other systems which were studied.

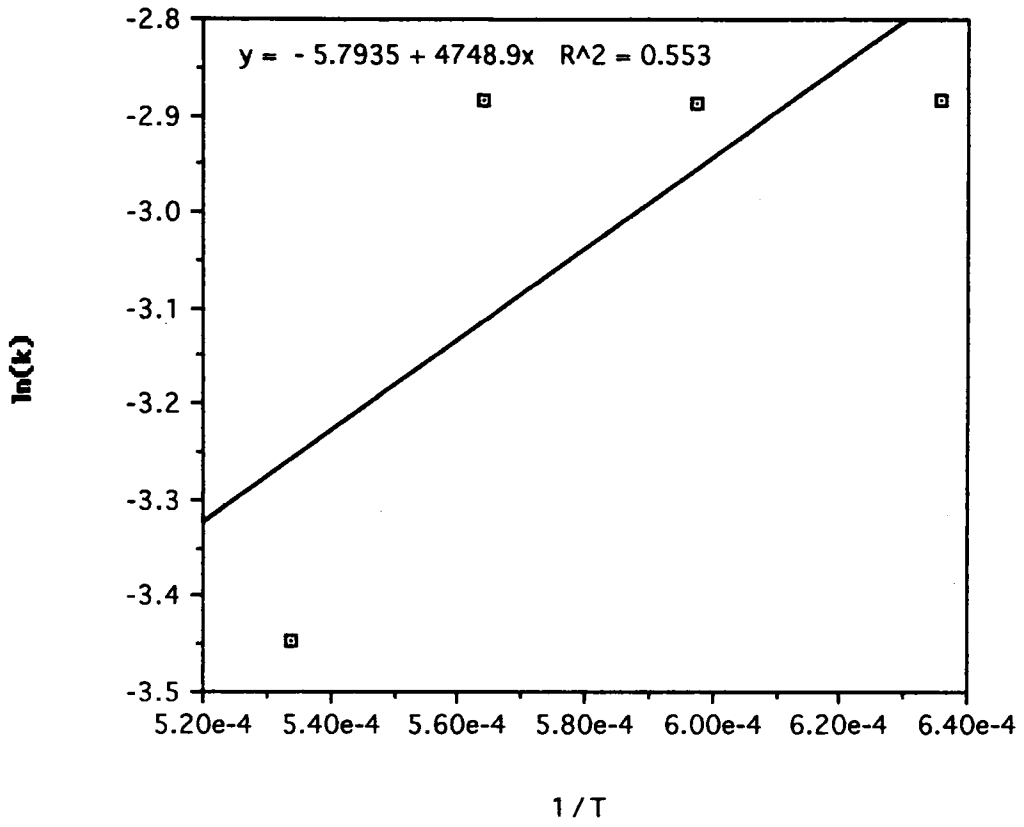

Figure 24: Activation Energy Determination for Copper System

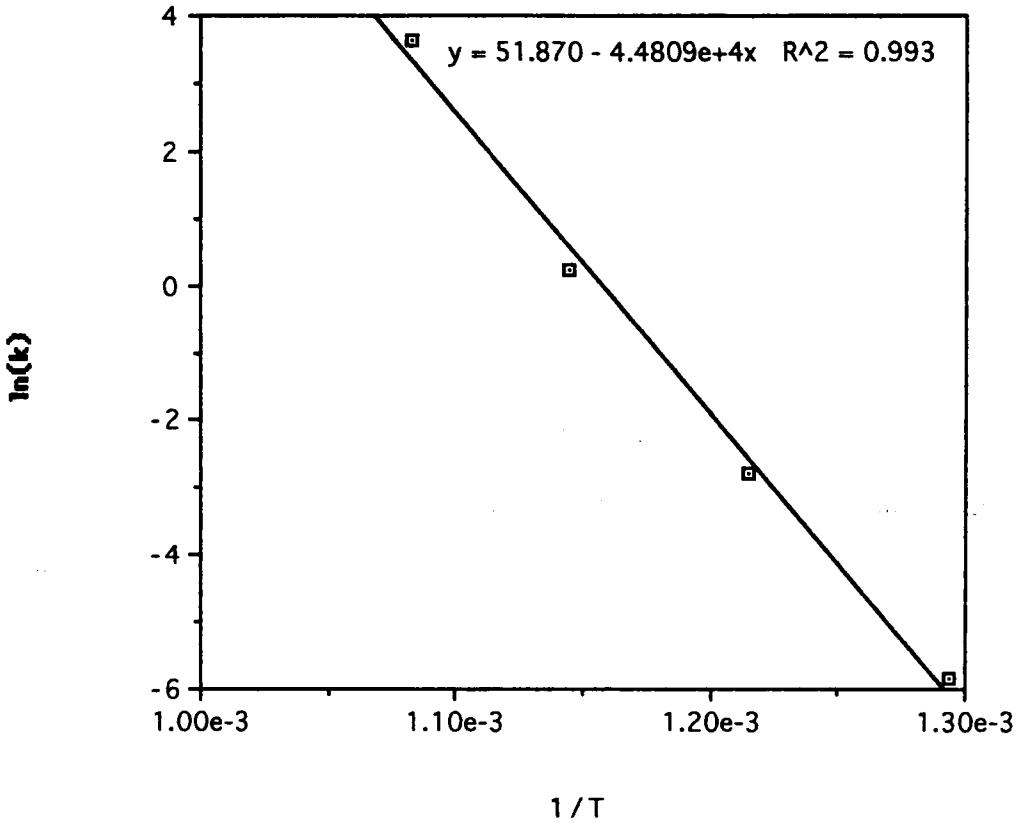

Figure 25: Activation Energy Determination for Zinc System

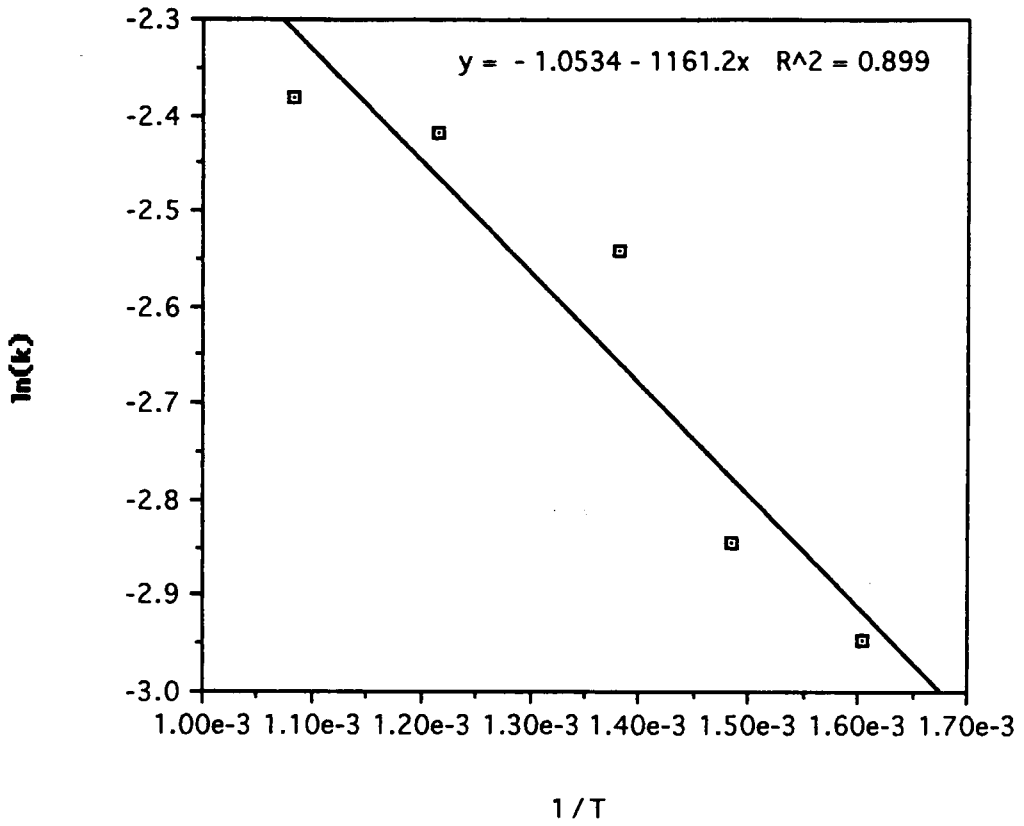

Figure 26: Activation Energy Determination for Tin System

Table 11: Experimentally Determined Activation Energies

System	Calculated Activation Energy, kJ/mole	Correlation Coefficient
Fe	---*	---*
Cu	-39	0.55
Zn	373	0.99
Sn	10	0.90

* Insufficient data for determination

The experimentally determined activation energy value for the zinc system is a factor of approximately 3 higher than the values given in the literature for catalytic decomposition of nitric oxide over metal oxide catalysts. It is approximately a factor of 5 higher than the values given in the literature for catalytic decomposition of nitric oxide over precious metal catalysts. Although the correlation coefficient for the activation energy plot for the zinc system is very good, post-run reactor disassembly revealed that the nitric oxide had reacted with the melt to form zinc oxide. No catalytic destruction can be inferred within this system.

The experimentally determined activation energy value obtained for the tin system (10 kJ/mole) is over an order of magnitude less than the values given in the literature for catalytic decomposition of nitric oxide over metal oxide catalysts and a factor of about six less than the literature values for decomposition of nitric oxide over precious metal catalysts. The correlation coefficient for the activation energy plot for the tin system is not very good. It appears likely that the data for the tin system is not linear. Based on the very low, experimentally determined activation energy for the system, it would be reasonable to draw the conclusion that this system was catalytically active for the decomposition of nitric oxide since the lowering of the activation energy is the criteria for demonstration of the catalytic nature of the melt system. The presence of tin oxide in the post-run reaction crucibles, however, is conclusive evidence that a reaction other than the simple decomposition of nitric oxide was taking place during the experiments involving tin. Based on this evidence it is not possible to declare the system catalytically active for the decomposition reaction of nitric oxide.

Thermal decomposition of nitric oxide within the injection lance occurred within all of the molten metal systems studied during this series of experiments. This is shown by assuming that the decomposition reaction is given by:

$$NO \rightarrow 1/2\ N_2 + 1/2\ O_2 \tag{23}$$

There is no net volume increase for the reaction. For a plug-flow reactor system with no net volume increase, the reactor design equation is given by [6]:

$$V = v_o \int_{C_A}^{C_{Ao}} \frac{dC_A}{-r_A} \tag{24}$$

Dividing both sides by v_o yields:

$$\tau = \int_{C_A}^{C_{Ao}} \frac{dC_A}{-r_A} \tag{25}$$

Since

$$-r_A = kC_A \tag{26}$$

equation (24) becomes:

$$\tau = \frac{1}{k} \int_{C_A}^{C_{Ao}} \frac{dC_A}{C_A} \tag{27}$$

For the injection lance system used for this series of experiments, an overall lance temperature profile was assumed for each steady state susceptor temperature. An example temperature profile is shown in Figure 27 for a melt temperature of 1600°C. An average lance temperature was calculated in order to determine the thermal decomposition reaction rate constant, k. Values of k were calculated using a literature [24] correlation:

$$k_{tot} = 7 \times 10^{12} e^{(150,000/RT)} + 4.8 \times 10^{20} T^{2.5} e^{(85,500/RT)} \qquad (28)$$

The integral limit C_A in equation (27) was iterated until the value of τ determined by this method converged to the value of the residence time as determined based on the known reactant feed rate, injection lance dimensions, and the average lance temperature. The results of these calculations are shown in Table 12. A plot of these results is given in Figure 28 and an overlay of the curve given in Figure 28 with the experimentally observed destruction curves for the (100% nitric oxide inlet concentration) iron and copper systems is given in Figure 29. The curves in Figure 29 indicate that at temperatures less than about 525°C, the metal systems exhibit destructions in excess of those predicted by thermal decomposition alone. This is consistent with what is expected based on the physical setup of the experimental reactor system. During the series of experiments, the alumina lance was initially lowered onto the top of the solid metal pellets and the reactant gases were introduced into the system during reactor heat-up. By allowing the reactant gases to pass over the heated metal, the gases were allowed to come into contact with a relatively high-surface-area, heated surface. This is responsible for the observed increase in nitric oxide destruction which was observed within this temperature range.

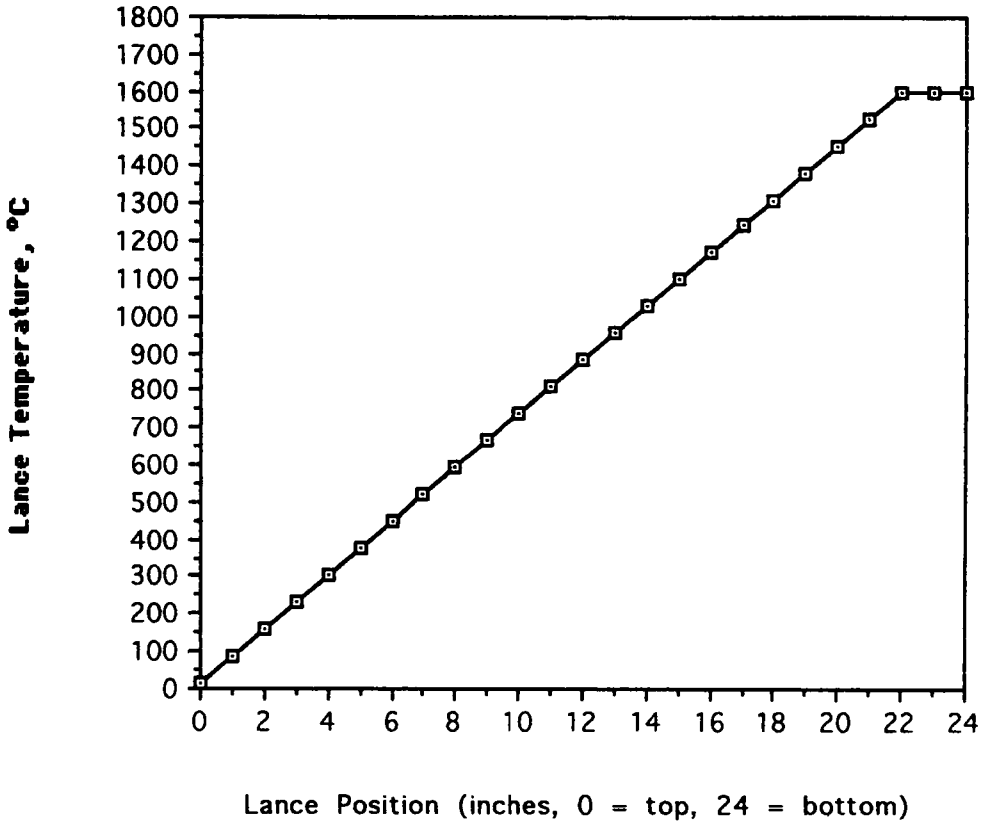

Figure 27: Example of Assumed Lance Temperature Profile

Table 12: Calculated Decomposition of Nitric Oxide in Injection Lance

Susceptor Temperature, °C	Assumed Average Lance Temp., °C	Reaction Rate Constant, k (1/s)	% Decomposition in Lance
600	337	0.0010	0.006
700	386	0.0092	0.055
800	445	0.085	0.51
900	495	0.44	2.62
1000	550	2.1	11.9
1100	604	8.2	38.6
1200	664	30.3	83.9
1300	713	79.4	99.1
1400	762	190	99.99
1500	822	490	>99.99*
1600	876	1069	>99.99*

* Integral would not converge

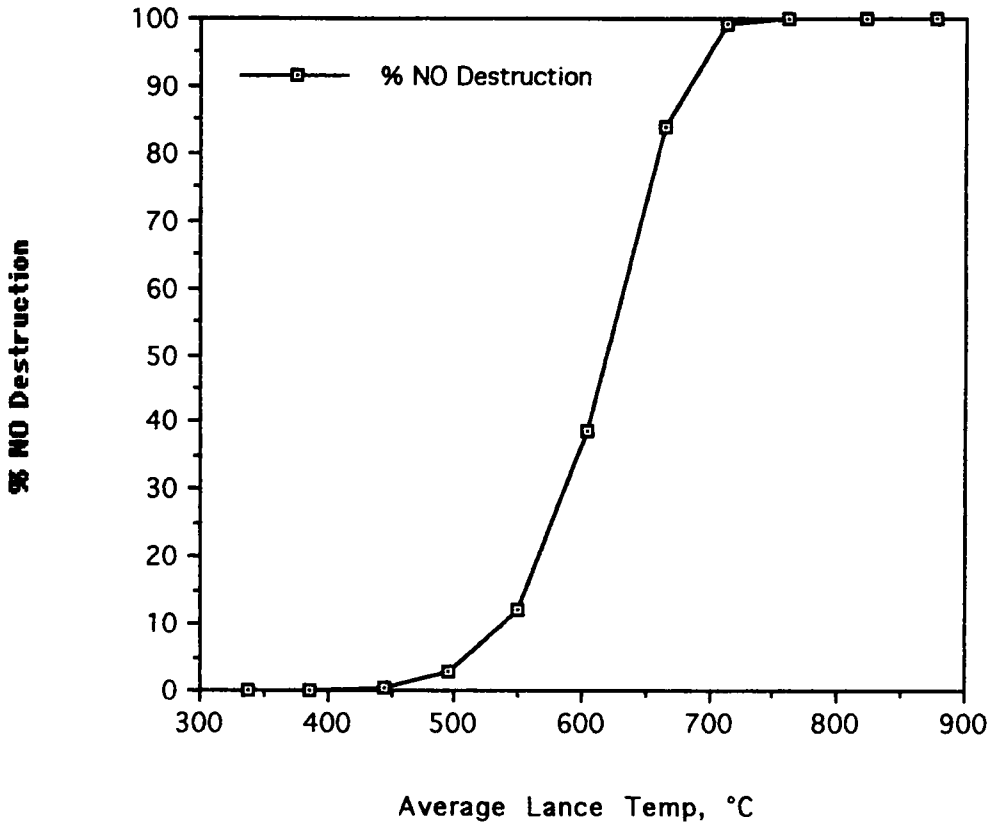

Figure 28: Predicted Decomposition of Nitric Oxide Within Injection Lance

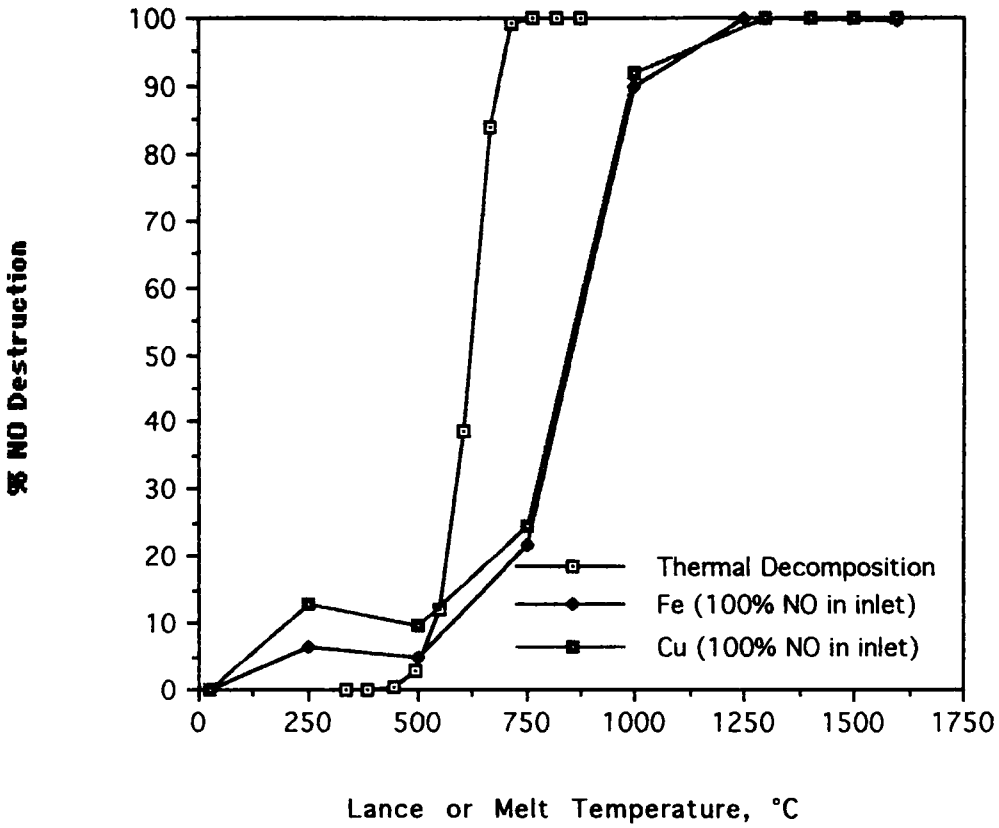

Figure 29: Comparison of Thermal Decomposition to Melt Systems

The injection lance was comprised of α-alumina (a low specific-surface-area form of Al_2O_3). Although there are reports in the literature [11,15,18] of catalytic enhancement of nitric oxide decomposition by activated γ-alumina (a much higher specific-surface-area form of Al_2O_3), the enhancement is questionable. Reported activation energies for catalytic decomposition of nitric oxide in γ-alumina systems are generally higher than the activation energy values reported [24,25,26,26] for the thermal decomposition of nitric oxide. Since α-alumina is, in general, even less active catalytically than activated γ-alumina, no catalytic enhancement to the decomposition of nitric oxide is attributable to the injection lance itself.

At temperatures exceeding 525°C, the expected amount of nitric oxide destruction due to thermal decomposition of the nitric oxide in the injection lance exceeded the observed results for both the iron and copper systems. A possible explanation for this is that the estimate of the average lance temperature used for calculating the thermal decomposition of nitric oxide may be incorrect.

Since neither the iron nor the copper system were molten until about 1600°C and 1100°C respectively, the effects of any destruction due to the melt would was unmeasurable because >99.99% of the nitric oxide was destroyed prior to reaching the melt. The sensitivity of the mass spectrometer used for these experiments was approximately ± 1%. No relevant conclusions concerning the catalytic activity of the liquid metals can be drawn from this series of experiments.

7. CONCLUSIONS

This series of experiments demonstrated the destruction of nitric oxide in several liquid metal reactor systems. The nature of the destruction which occurred within the reactor systems was investigated. An analysis of the experimental data revealed the following:

1) The destruction of nitric oxide in the iron and copper melt systems occurred by thermal decomposition of the nitric oxide within the injection lance.
2) The destruction of nitric oxide in the tin and zinc melt systems occurred both by thermal decomposition of the nitric oxide within the injection lance and by reaction of the nitric oxide with the melts.
3) No catalytic enhancement of the decomposition of nitric oxide could be inferred for any of the melt systems.

The following changes to the experimental approach used in this study should be used for any future attempts to determine the catalytic activity of liquid metals:

1) A gas phase reagent with a higher temperature tolerance for thermal decomposition should be used.
2) A reagent should be selected which does not react with the liquid metal.
3) Bottom injection into the melt should be used in order to prevent exposure of the reagent to a too high temperature within the injection mechanism.
4) A more detailed analysis of the mass and heat transfer characteristics of the system should be completed prior to experimentation.

REFERENCES

References

[1] HSC Chemistry, Okamptu Research, Okamptu, Sweeden, 1993

[2] Konduri, R. and Kyrlidis, A., "CEP Gas Phase Product Quality Scaleup Criteria," Interim Progress Report Draft, Molten Metal Technology, Inc., Fall River, MA, 1996

[3] Deen, W.M., Analysis of Transport Phenomena, Department of Chemical Engineering, MIT, Oxford University Press, Cambridge, MA, 1996

[4] Perry, R.H. and Green, D., Perry's Chemical Engineer's Handbook, 6th ed., McGraw-Hill, New York, 1985

[5] Beer, Sylvan Z., Liquid Metals: Chemistry and Physics, M. Dekker, New York, 1972

[6] Fogler, S.H., Elements of Chemical Reaction Engineering, 2nd ed., Prentice-Hall Inc., New Jersey, 1992, pp.67, 190-286

[7] Li, Y., and Hall, W.K., *J. Catal.* **129**, 202, (1991)

[8] Sourirajan, S., and Blumenthal, J.L., Proc. Second Inter. Cong. on Catalysis, Vol. II, p.2521, Paris, 1960

[9] Shelef, M., and Kummer, J.T., Chemical Engineering Progress, Symposium Series 67 (no.115), 74 (1971)

[10] Wise, H., and French, M.F., *J. Chem. Phys.* **20**, 1 (1952)

[11] Fraser, J.P., and Daniels, F., *J Phys. Chem* **62**, 22 (1958)

[12] Yuan, J., et.al., *J. Chem Phys.* **63**, 952 (1959)

[13] Taylor, F.R., *Air Pollution Foundation Report No. 28*, (1959)

[14] Sakaida, R.G., et.al. *AIChE Journal 7*, 658 (1961)

[15] Peters, M.S., AEC Report No. TID-18423 (1963)

[16] Wilkstrom, L.L., and Nobe, K., *I&EC Proc. Des. and Devel.*, **4**, 191 (1965)

[17] Yur'eva, V.V., et.al., *Kinetika i Kataliz* **6**, 1041 (1965)

[18] Winter, E.R.S., *J. Catal.* **22**, 158 (1971)

[19] Green, T.E., and Hinshelwood, C.N., *J. Chem Soc.* **129**, 1709 (1926)

[20] Bachman, P.W., and Taylor, G.B., *J, Phys. Chem.* **33**, 447 (1929)

[21] Zawadzki, J., and Perlinski, G., *Comptes Rend.* **198**, 260 (1934)

[22] Shelef, M., et.al., *Atm. Environ.* **3**, 107 (1969)

[23] Amirnazmin, A., et.al., *J. Catal.* **30**, 55 (1973)

[24] Freedman, E. and Daiber, J.W., *J. Chem. Phys.* **34**, 4 (1961)

[25] Kaufman, F., and Kelso, J.R., *J. Chem. Phys.* **23**, 1709 (1954)

[26] Feinmore, C.P., and Jones, G.W., *J. Phys. Chem.* **61**, 654(1957)

[27] Mallard, W.G., et al, *NIST Chemical Kinetics Database*, Version 6.01, Gaithersburg, MD, 1994

VITA

Christopher Bible was born on a snowy day in January, 1968, in Fort Wayne, Indiana. During the first year of his life he moved, with his family, to East Tennessee where he was raised with a spirit of practicality and hard work. After graduation from high-school in 1985, he entered the U.S. Army in order to finance his undergraduate education. After a three year tour of duty with a field-artillery unit in Europe, Mr. Bible returned to the United States and entered the University of Tennessee Chemical Engineering undergraduate program. Mr. Bible obtained a Bachelor of Science degree in Chemical Engineering and went to work, initially as a research and development engineer, then as a consulting engineer.

Mr. Bible's work experience to date includes nearly six years experience in research, development, and design of mixed-waste and air pollution treatment systems. He also has significant hands-on process development and operational experience in the areas of air pollution control catalytic systems and mixed and hazardous waste treatment systems. He has performed both conceptual and detailed designs of transuranic, mixed-waste treatment systems and air pollution abatement catalytic systems and has supervised the construction and deployment of high-temperature bench and pilot-scale mixed waste treatment systems. He has also been involved with the commercialization and start up of novel catalytic air pollution control technology and mixed-waste treatment systems. Additionally, he has performed technical reviews and analyses for Department of Energy sponsored feasibility studies involving transuranic waste treatment systems and radionuclide contaminated scrap metal recycling.

While working full-time, Mr. Bible entered the University of Tennessee Chemical Engineering Graduate Program. He obtained the degree of Master of Science in Chemical Engineering in December, 1998.